

https://dspace.org/

Trabecular morphology of humeri with the Supratrochlear Aperture (STA) and characteristics of the tissue crossing the STA

Pillay, Shayla Kohrika

2020

https://hdl.handle.net/10539/31954

Downloaded from a DSpace repository. https://dspace.org/

Trabecular morphology of humeri with the Supratrochlear Aperture (STA) and characteristics of the tissue crossing the STA



Shayla Kohrika Pillay

A dissertation submitted to the Faculty of Health Sciences, University of the Witwatersrand, Johannesburg, in the fulfilment of the requirements for the degree of Master of Science in Medicine

FACULTY OF HEALTH SCIENCES

UNIVERSITY OF THE WITWATERSRAND, JOHANNESBURG

2020

DECLARATION

I, Shayla Kohrika Pillay (student number: 481830), am a registered student for the degree of Master of Science in Medicine in the academic year of 2019 at the University of the Witwatersrand, Johannesburg.

I hereby declare the following:

- This work has not been submitted before for any degree or examination at any other university
- That this dissertation entitled "Trabecular morphology of humeri with the Supratrochlear Aperture (STA) and characteristics of the tissue crossing the STA" is my own unaided work except where I have explicitly stated otherwise.
- I am aware that plagiarism is wrong and have followed the conventions in referencing the thoughts and ideas of others



Shayla Kohrika Pillay

19 August 2020 at Randburg, Johannesburg

ABSTRACT

The supratrochlear aperture (STA) of the humerus is the opening that forms when the septum separating the coronoid and olecranon fossae is perforated. While the aetiology is unknown, one study suggested that articulation of the ulnar coronoid process with its respective fossa may cause septal resorption to form the STA. Conversely, recent findings implicated a longer olecranon process. This study aimed to test the validity of these two suggestions using cadaveric samples as well as to investigate the differences in the internal bone morphology in individuals with and without the STA to determine whether the STA may form due to incomplete bone remodelling.

Bone samples were taken from 30 cadavers with equal numbers in the STA category, controls with a thick (opaque) septum or with a thin (translucent) septum and fixed in paraformaldehyde, decalcified and processed for histological assessment. The posterior aspects of the samples were marked to differentiate the coronoid (anterior) from the olecranon (posterior) side. Sections (5µm thick) were cut with a microtome and stained with H&E for morphological assessment, Rapid One-Step Mallory Heidenhain to identify the connective tissue structure and Picrosirius Red to analyse the collagen types found in the section. Images of the sections were captured using the Olympus BX63 Fluorescence Microscope. Area, length and width measurements were taken to measure bone resorption. Area measurements of the connective tissue on translucent sections were taken on anterior and posterior surfaces. A gradient was plotted onto each section, for the opaque and translucent septum sections to measure the difference in density of bone from anterior to posterior.

Additionally, 30 paired humeri belonging to females of African descent between the ages of 18 and 50 years were selected from the Raymond A Dart Collection of Human Skeletons. These comprised of 15 bilateral humeri with the STA and 15 bilateral humeri without the STA. Humeri were scanned using a Nikon XTH 225/320 LC dual-source industrial Micro-CT scanner. Measurements from the reconstructed images included the bicondylar breadth, bone to total volume (BV/TV), trabecular number (TbN), thickness (TbTh) and spacing (TbSp). These measurements aided in determining whether there were differences in bone volume by STA status.

Histological analysis showed increased occurrence of connective tissue found on the posterior aspect of translucent septum sections compared to that on the anterior aspect.

Similarly, there was an increased percentage of bone found on the anterior aspect compared to the posterior aspect of the section in translucent septum sections. Significant differences were found in the BV/TV, TbN and TbSp, in the proximal region on the right in humeri with the STA. Therefore septal resorption occurs primarily from the posterior aspect and the differences in trabecular bone may have resulted from the overactivity of osteoclasts.

DEDICATION

To my godmothers Cheryl Deline Phillips (1955 – 2004) and Wendy Lorraine Ruthanum (1959 – 2014) whose presence was always felt.

ACKNOWLEDGEMENTS

I would like to thank my funder the NRF Thuthuka fund. I am grateful to Mrs Hasiena Ali for the instrumental training in histological and immunohistochemical staining procedures. I would like to thank Mr Kudakashwe Jakarta for his invaluable assistance in the micro-focus X-ray computed tomography scanning. I would like to further extend my deepest gratitude to my supervisors Professor Lynne Schepartz for her guidance, support and understanding throughout this journey, Professor Robert Ndou, whose insight and knowledge into the subject matter steered me through this research and Dr Diana Pillay whose assistance and advice allowed my studies to go the extra mile. I would like to thank Dr Desiré Brits for constantly motivating me and shaping me into a better individual as well as Dr Temitope Esan whose advice filled me with confidence whenever it was needed. I am grateful to my family, particularly my parents, Reg and René who were pillars of strength, guidance and patience, especially when trying to understand what my work entails. To my sisters, Megan and Kineshea, thank you for always supporting me no matter what, motivating me to always do better, and especially for putting up with me in my crazy moments. I am grateful to my brothers-in-law, John and Jonathan for always discussing my research, even if you didn't want to, thanks for feigning "genuine" interest. Thank you to my nieces, Amia and Elliah whose exuberance and inquisitive nature encouraged me throughout this journey; and to my godson Kayden who never failed to discuss the meaning of life with me. To my friends who have become my family throughout the years, Kyrtania Pather, Sashrika Pillay and Joseph Tewson thank you for continually challenging me and being so annoyingly supportive. Thank you to my friends and fellow postgraduate students, Nicholas Bacci, Ursula Mariani and Vaughan Perry for inspiring me every day and always contesting my thought process.

Table of Contents

Item	Page
Declaration	II
Abstract	III
Dedication	V
Acknowledgements	VI
Table of contents	VII
List of abbreviations	X
List of figures	XII
List of tables	XIV
Chapter 1: Introduction	1
1.1 The elbow joint	1
1.2 The Septum and the STA	3
1.2.1 Studies of STA prevalence	4
1.2.2 Formation of the STA	5
The mechanical theory	5
The genetic theory	6
1.3 Histological aspects and the STA	6
Connective tissue	7
Collagen	7
1.4 Bone	9
1.4.1 Bone structure	9
1.4.2 Bone remodelling	12
Cellular components & microscopic structure of bone	12
Remodelling	12
1.4.3 Bone mineral density	15
1.4.4 Biomechanics of bone	16
Wolff's Law and Young's Modulus	16
Mechanics of materials	17
Collagen orientation	17
1.5 Bone imaging modalities	18
1.5.1 Imaging modalities used for the evaluation of bone mineral Density	18
Dual X-ray absorptiometry	18
Quantitative computed tomography	18
1.5.2 Imaging modalities used for the evaluation of the bone quality	19
Radiography	19
Magnetic resonance imaging	19
Micro-CT	19
1.6 Clinical significance of the STA	20
1.7 Research questions	20
1.8 Aims	21
1.9 Objectives	21
Chapter 2: Materials and methods	22
2.1 Cadaveric histological tissue analysis	22
2.1.1 Sample	22
2.1.2 Dissection techniques for tissue collection	23
Identification of the STA	24
Tissue harvesting	25

Bone decalcification 26
Tissue processing 27
Paraffin wax embedding 27
Microtome sectioning 27
2.1.3 Staining of sections 28
Haematoxylin and Eosin staining 28
Rapid one-step Mallory-Heidenhain staining 28
Picro sirius red staining 29
2.1.4 Imaging of sections 29
2.1.5 Measurements for the resorption of bone 30
2.1.6 Measurements for bone area – anterior vs. posterior 32
2.2 Micro-ct bone structural analysis 33
2.2.1 Sample of dry bone specimens 33
2.2.2 Methods 33
Measurements of the internal structure of the humerus 33
Reconstruction of the slices to create a 3D image 34
Trabeculae morphological parameters 35
2.3 Data analysis 36
2.4 Ethics 37
Chapter 3: Results 38
3.1 Histomorphometric analysis of the STA 38
3.1.1 Tissue composition of sections 38
3.1.2 Quantitative results 41
Measurement repeatability 41
Outliers 41
Normality 41
Descriptive statistics 42
Measurements of bone volume 45
Measurement of bone volume – anterior vs. posterior 46
Measurement of connective tissue area 51
Anterior vs. Posterior connective tissue area 53
3.2 Morphometric properties of humeri with and without the STA 54
3.2.1 Bicondylar breadth 54
3.2.2 Bone to total bone volume (BV/TV) 54
3.2.3 Trabecular thickness (TbTh) 55
3.2.4 Trabecular number (TbN) 56
3.2.5 Trabecular spacing (TbSp) 57
Chapter 4: discussion 59
4.1 Tissues crossing the STA 59
Bone volume 60
Connective tissue area 60
Anterior vs posterior connective tissue area 61
4.2 Internal osseous morphology of humeri 61
Bicondylar breadth 61
Trabecular bone 61
Chapter 5: Conclusions 63
5.1 Limitations 63
5.2 Recommendations 63
References 65
Appendices 73

Appendix A: Reagents and Equipment used 73
Appendix B: 10% neutral buffered formalin 75
Appendix C: 10% Formic citric acid decal fluid and saturated ammonium Oxalate 76
Appendix D - Tissue processing 77
Appendix E – Haematoxylin and Eosin staining procedure 78
Appendix F – Rapid one-step Mallory Heidenhain staining procedure 79
Appendix G – Picrosirius red staining procedure 80
Appendix H – Anterior vs. posterior measurement gradient on imageJ 81
Appendix I – Analysis on VG Studio Max 82
Appendix J – Ethics waiver 84
Appendix K – Turn-it-in report 85

List of Abbreviations

%: per cent

°: degrees

°C: degrees Celsius

2D: Two-dimensional

3D: Three dimensional

cm: centimetres

kV: kilovolts

ml: Millilitre

mm: millimetre

nm: nanometre

µm: micrometre

µCT: Micro-computed tomography

ANOVA: Analysis of variance

BMD: Bone mineral density

BV: Bone volume

BV/TV: Bone to total volume

DXA: Dual X-ray absorptiometry

GPa: Gigapascal

H_2O_2: Hydrogen peroxide

H & E: Haematoxylin and eosin

MRI: Magnetic resonance imaging

PTH: Parathyroid hormone

QCT: Quantitative computed tomography

SD: Standard deviation

STA: Supratrochlear aperture

TbN: Trabecular number

TbSp: Trabecular spacing

TbTh: Trabecular thickness

LIST OF FIGURES

Figure	Title	Page
Figure 1.1	The three components of the elbow joint	2
Figure 1.2	The fossae of the distal humerus and the STA region	3
Figure 1.3	Shapes of the STA	4
Figure 1.4	Humerus indicating different parts of the bone	9
Figure 1.5	The bone remodelling cycle	14
Figure 2.1	Dissection of the elbow joint in preparation for tissue harvesting	23
Figure 2.2	Portable dental X-ray machine positioned in the custom-designed table	24
Figure 2.3	X-ray scans of the humerus indicating STA presence, a translucent septum and an opaque septum	25
Figure 2.4	U-shaped metal clip demarcating the STA boundaries in a cadaver and on a radiograph	25
Figure 2.5	Thin wire indicating the point of bisection to ensure the area of the STA was represented when cutting sections on the microtome	26
Figure 2.6	Sequence of stains of the sections	28
Figure 2.7	Diagram of the measurements taken from bone sections with the STA, the control group with an opaque septum and translucent septum	31
Figure 2.8	Area measurements taken to compare the bone area on the anterior and posterior aspects of the bone section.	32
Figure 3.1	STA (composite image) stained with rapid one-step mallory heidenhain	38
Figure 3.2	Opaque septum sample (composite image) stained with rapid one-step mallory heidenhain	39
Figure 3.3	Translucent septum sample (composite image) stained with rapid one-step mallory heidenhain	33
Figure 3.4	Translucent septum and STA present sections (composite image) stained with picrosirius red	40
Figure 3.5	Opaque septum sample (composite image) stained with rapid one-step mallory heidenhain	45
Figure 3.6	Graphical depiction of the distribution of bone in translucent septum sections when divided into 20^{th} percentiles.	47
Figure 3.7	Graphical depiction of the mean percentage of area occupied by bone on translucent septum sections, divided into 20^{th} percentiles.	48
Figure 3.8	Graphical depiction of the distribution of bone in opaque septum sections when divided into 20^{th} percentiles.	49
Figure 3.9	Graphical depiction of the mean percentage of area occupied by bone on opaque septum sections, divided into 20^{th} percentiles.	50
Figure 3.10	Graphical representation of the difference between opaque and translucent septum sections in the measurement of bone area, comparing anterior to posterior density.	51
Figure 3.11	Translucent septum sample (composite image) stained with picrosirius red indicating connective tissue formation on the anterior (A) and posterior (B) aspects	52
Figure 3.12	Graphical representation of the difference between the connective tissue area found on the anterior and posterior aspects of translucent and opaque septum sections.	53

Figure 3.13	Graphical depiction of the left and right bicondylar breadth measurements indicating the difference between bone when the STA was present and bone when the STA was absent	54
Figure 3.14	Trabecular morphometric measurement of bone volume to total volume (BV/TV) compared according to STA status.	55
Figure 3.15	Trabecular morphometric measurement of the trabecular thickness (TbTh) compared according to STA status.	56
Figure 3.16	Trabecular morphometric measurement of trabecular number (TbN) compared according to STA status.	57
Figure 3.17	Trabecular morphometric measurement of trabecular spacing (TbSp) compared according to STA status	58

LIST OF TABLES

Table	Title	Page
Table 2.1	Cadaveric samples	23
Table 2.2	Parameters for the µCT scans	33
Table 2.3	Definition and description of outcomes from µCT scans	35
Table 3.1	Lin's concordance correlation coefficients of reproducibility (P_c) for intra- and inter-observer repeatability for histomorphometric measurements	42
Table 3.2	Descriptive statistics of histomorphometric measurements	44
Table 3.3	Results of the independent samples t-tests for measurements of bone area	46
Table 3.4	Results of the independent samples t-tests for measurements for connective tissue area	52

Chapter 1

Introduction

There are many aspects of the elbow joint that are part of the canon of morphological anatomy, yet some features are not fully understood. The supratrochlear aperture (STA) is one such feature. The STA is a variable perforation of the septum between the olecranon and coronoid fossae of the humerus. The STA has been a subject of study for over a century, yet its aetiology and many attributes of bones with this feature remain unknown. Ndou & Schepartz (2016) described some of the anatomical characteristics of humeri and ulnae that are correlated with STA status. The role of the internal bone structure is less understood. For example, how does the internal morphology of humeri bearing the STA differ from those without it? This study investigates 1) variation in bone mineral density, 2) the volume, thickness and size of trabeculae, and 3) the histological characteristics of the tissues in the STA region of humeri with and without the STA.

1.1 The elbow joint

As the STA forms on articular surfaces of the elbow joint, an understanding of the basic anatomy of that joint is important for STA research. The elbow joint (Fig. 1.1) is classified as a synovial trochoginglymoid joint as it allows for flexion, extension, pronation and supination of the forearm (Morrey *et al.,* 2018). It is formed by the articulation of the humerus, radius and ulna and connects the arm to the forearm (Morrey *et al.,* 2018; Drake *et al*., 2019). The articulating surfaces of the elbow consist of three separate portions (Fig 1.1) viz the humeroulnar joint, involving the trochlear notch of the ulna and the trochlea of the humerus; the radiocapitellar joint involving the head of the radius and the capitulum of the humerus; and lastly the proximal radioulnar joint that is located distal to the other articulations within the same joint capsule and is formed by the articulation between the head of the radius and the radial notch of the ulna (Morrey *et al.,* 2018; Drake *et al*., 2019). Of these, the humeroulnar joint is of particular importance because the articular surfaces include the anterior coronoid and the posterior olecranon fossae of the distal humerus. These together constitute the region of STA formation (Figure 1.2). The coronoid and olecranon fossae are bordered by the small medial and the stronger lateral bony supracondylar columns. The difference in the size of these structures is important because the smaller medial column may

be vulnerable to fracture from the insertion of osteological elements during flexion as well as during surgical procedures (Morrey & An, 2005; Chalmers & Chamberlain, 2017).

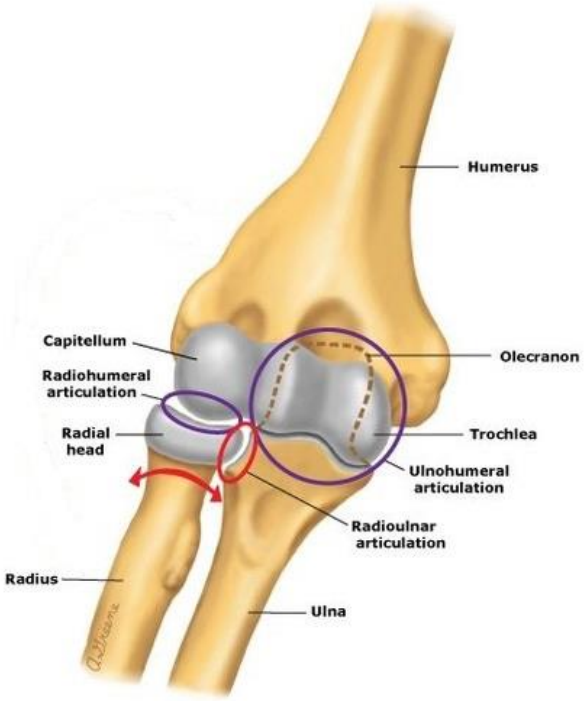


Figure 1.1: The three components of the elbow joint. From "Elbow Flashcards" by Quizlet (2019). https://quizlet.com/ca/ 274538455/elbow-flash-cards/. Circled are the three articulations of the elbow joint. The dotted line indicates the position of the olecranon process in extension on the posterior surface of the elbow.

The elbow is primarily a hinge joint allowing for flexion and extension although there are pronation and supination produced by the radioulnar joints (Drake *et al.*, 2019). During elbow flexion, the actions of the brachialis, biceps brachii, and brachioradialis muscles allows for the ulnar coronoid process to insert anteriorly into the coronoid fossa of the humerus (Rooker *et al.*, 2016; Morrey *et al.*, 2018; Drake *et al.*, 2019). In extension, the ulnar olecranon process moves posteriorly into the olecranon fossa through the actions of the triceps and anconeus muscles (Rooker *et al.*, 2016; Morrey *et al.*, 2018).

The trochlea is covered by hyaline cartilage over an arc of ± 320° (Daniels, 1998) while the trochlear notch creates an arc of ± 180°. Typically these arcs of motion are limited by the geometry of the joint surfaces, the surrounding bone and the soft tissue. In normal circumstances elbow flexion ranges from 0° to ± 150° (Rooker *et al.*, 2016). Extension of the

elbow joint is restricted by the olecranon process within the olecranon fossa and the tension of the posterior soft tissue of the capsule and muscles. Flexion, both active and passive, is limited beyond 145° by the anterior bulk of the flexor muscles and the contraction of the triceps muscle (Rooker *et al.,* 2016; Morrey *et al.,* 2018) Passive flexion is further limited by the radial head impacting the radial fossa and the coronoid process impacting the coronoid fossa (Morrey *et al.,* 2018). The elbow joint is one of the most concordant joints of the musculoskeletal system in that it primarily relies on the soft tissue and surrounding articular surfaces to provide stability and maintain the joint function and loading configuration (Morrey & An, 2005).

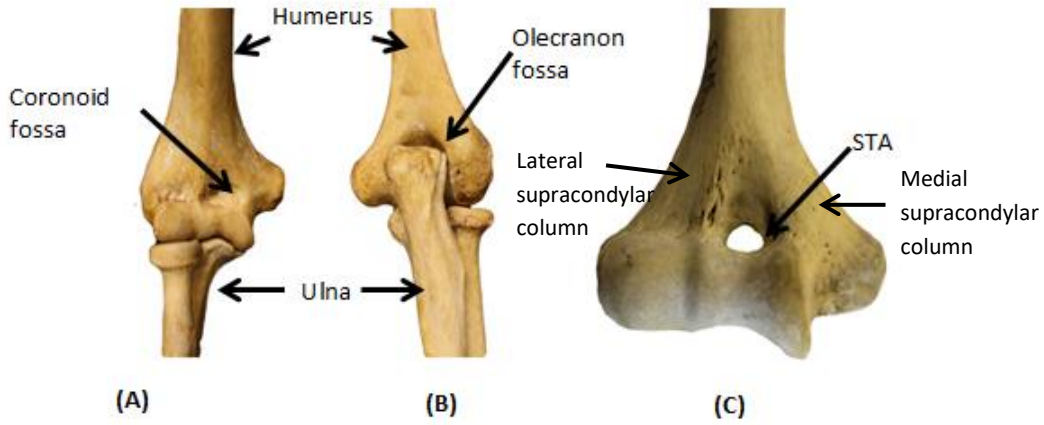


Figure 1.2: The fossae of the distal humerus and the STA region. (A) Showing the coronoid fossa anteriorly, (B) olecranon fossa posteriorly and (C) STA. Image courtesy of R Ndou**.**

1.2 The bony septum and the STA

A thin bony structure or septum typically separates the olecranon and coronoid fossae. This septum varies between 0.5 cm and 1 cm in thickness (Krishnamurthy *et al.,* 2011). Ndou (personal communication, 2015) observed that the septum exists as two separate anterior and posterior bony plates that usually fuse but are perforated to form the STA (Fig. 1.2C) (Paraskevas *et al.,* 2010; Krisnamurthy *et al.,* 2011; Diwan *et al.,* 2013; Ndou *et al.,* 2013; Patel *et al.,* 2013). The STA is also referred to as the supratrochlear foramen (Paraskevas *et al.,* 2010; Krishnamurthy *et al.,* 2011), the septal aperture, the intercondylar foramen or the olecranon foramen (Paraskevas *et al.,* 2010). It is best characterised as an aperture,

specifically due to the difference in anatomical characteristics from a foramen (Ndou *et al.*, 2018). A foramen is defined as a passageway for vessels whereas apertures are openings in bone (Drake *et al.*, 2019). No known anatomical structures pass through the STA and some studies report the STA being covered by a tissue membrane (Nayak *et al.*, 2009). However, Ndou and colleagues (2018) identified that connective tissue occupies the area of the STA. The histology of this tissue will be discussed in detail in the following section.

The STA appears in many forms (Fig. 1.3) with the oval shape being the most prevalent (Mays, 2008; Krishnamurthy *et al.*, 2011; Diwan *et al.*, 2013; Ndou *et al.*, 2013; Patel *et al.*, 2013).

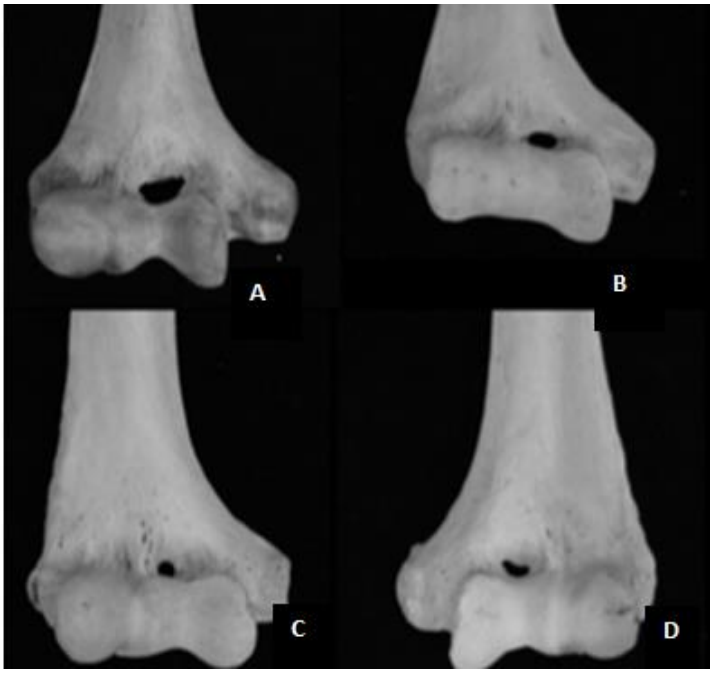


Figure 1.3: Shapes of the STA. A: Triangular. B: Oval. C: Round. D: Irregular. Image courtesy of Ndou *et al* (2013).

1.2.1 Studies of STA prevalence

STA prevalence varies according to population and study results differ depending on the sample evaluated. In one study of the Greek population, it was as low as 0.3% (Papaloucas *et al.*, 2011) while Paraskevas *et al.* (2010) found a prevalence of 15.8%. Trotter (1934) stated that STA prevalence is higher in non-European ancestry populations. However, the Australian European ancestry population has a prevalence of 46.5% (as cited in Mahajan, 2011), similar to the Sotho group of South Africa with a 41% prevalence (Ndou *et al.*, 2013).

Among modern Asians (Indians, Japanese, Korean and Chinese), the STA prevalence ranges between 9 - 32%, being highest in Indians (23-32%) (Krishnamurthy *et al.*, 2011; Diwan *et al.*, 2013; Patel *et al.*, 2013). Akabori (1934) reported a prevalence of 9 -18% in the Japanese population and 11% overall in Koreans. Among the Chinese, the overall prevalence is reported to be 17.5% (Ming-Tzu, 1935). Interestingly, Hirsh (1927) found a prevalence of 58% in the Arkansas Native American population which is the highest reported for a group with northern Asian roots.

Worldwide, the STA is more frequently found on the left humerus. There are incidences of bilateral occurrence, but these typically characterise less than half of the cases (Mays, 2008; Krishnamurthy *et al.*, 2011; Diwan *et al.*, 2013; Ndou *et al.*, 2013; Patel *et al.*, 2013). Ndou *et al.* (2015) indicated that the STA occurred unilaterally almost four times more frequently on the left side (13.9%) compared to the right side (3.5%). STA bilateral expression was found for 15.1% of the South African with twice as many females affected as males.

The STA is more frequent in females in almost all populations that have been studied (Akabori, 1934; Trotter, 1934; Ming-Tzu, 1935; Mays, 2008; Krishnamurthy *et al.*, 2011; Diwan *et al.*, 2013; Ndou *et al.*, 2013; Patel *et al.*, 2013). The Japanese population presented with a higher incidence in females (20.6%) compared to males (13.5%). The Korean population exhibited STA presence in 15% in females and 6.9% in males (Akabori, 1934). In the Chinese population, STA prevalence in females was 27.3% compared to 7.8% in males (Ming-Tzu, 1935). Ndou *et al.* (2015) found that the STA was expressed in 19.5% of females compared to 13% of males in the overall South African population.

Another important characteristic of the STA is its absence in juveniles prior to the epiphyseal union of the distal humerus (Mays, 2008). This observation holds for all populations and should be factored into explanations of STA formation.

1.2.2 Formation of the STA

Although the aetiology of the STA remains unknown, two main theories attempt to explain its formation (Mays, 2008; Krishnamurthy *et al.*, 2011; Ndou *et al*., 2013).

The mechanical theory

The mechanical theory suggests that aperture formation occurs as a result of septum resorption in response to forces generated from the actions of the ulnar processes during elbow flexion and extension. Mays (2008) proposed that the septal resorption rate is higher

on the anterior surface, indicating that impingement of the septum occurs primarily due to the action of the coronoid process during extreme flexion.

Krishnamurthy *et al.* (2011) argued that if the mechanical theory were to cause aperture formation then the STA would be more frequently found in males rather than females and would occur more frequently on right humeri. This explanation is based on the majority of people being right-handed and the division of labour between males and females. The greater loads on the elbow that are generated in men (and in some populations) are largely due to differences in bone dimensions (Duan *et al.*, 2005; Wang *et al.*, 2005). Therefore the formation and prevalence of the STA are dependent on factors such as the smaller size of female bones, which may predispose them to aperture formation, whereas a thicker humeral septum in males may resist the pressure of elbow flexion and extension (Mays, 2008).

Ndou & Schepartz (2016) examined the morphological characteristics of STA bearing bones in South African groups to evaluate the mechanical theory. In light of the physical constraints on flexion and extension, as mentioned above, Ndou & Schepartz (2016) argued that the presence of muscles in the anterior compartment of the arm would restrict active and passive flexion (c.f. Kapandji, 1982) and therefore limit the coronoid process interaction in STA formation. Ndou & Schepartz (2016) demonstrated that a significantly longer olecranon process, but not a longer coronoid process is associated with the STA. Additionally, they confirmed that smaller bones are more prone to STA formation.

The genetic theory

The genetic theory suggests that the STA is an inherited characteristic. The dissimilarity in the frequency of bilateral and unilateral occurrences between populations is argued to be evidence that STA aetiology has a genetic component (Glanville, 1967). Factors such as a disturbance in bone development have been attributed to genetic variation leading to STA formation (Koyun *et al.*, 2011).

1.3 Histological aspects and the STA

Ndou and colleagues (2018) identified that the tissue crossing the STA is dense regular connective tissue. Formation of the STA may occur due to incomplete bone remodelling. This may be from the lack of hydroxyapatite incorporated during the formation phase of remodelling (Ndou, 2015; Ndou *et al.,* 2018). Therefore, knowledge of the presence of the types of collagen present may contribute to the understanding of STA formation. Furthermore, understanding of bone resorption on the anterior and posterior aspects of the septum may further the knowledge of STA formation

Connective tissue

Connective tissue is composed of collagen, reticular and elastic fibres. Distribution of these fibres is connective tissue type-dependent, resulting in the predominant fibre type being responsible for specific tissue properties (Ushiki, 2002; Paulsen 2010). Connective tissue not only functions as a mechanical support for other tissues but also as an avenue for communication and transport among other tissues. Classification of connective tissue is based on composition, i.e. the proportion of cellular and extracellular components (Ushiki 1992, Ushiki, 2002; Kierszenbaum & Tres, 2012).

a. Loose connective tissue has a relatively large proportion of ground substance or cells. It lacks fibrous reinforcement that characterises dense connective tissue. Loose connective tissue is easily distorted, permitting tissues on either side to move freely with respect to one another (Kierszenbaum & Tres, 2012).
b. Dense connective tissue has a high density of extracellular fibres and relatively smaller proportions of ground substance and cells (Kierszenbaum & Tres, 2012). Dense collagenous connective tissue is found wherever tensile strength of collagen is of paramount importance such as in skin, tendons, ligaments and organ sheaths, whereas dense elastic connective tissue is found where elastin is of paramount importance such as in the aorta (Marieb, 2009). Dense connective tissue is divided into regular and irregular forms, depending on the fibre orientation:
    i. Dense regular connective tissue has fibres aligned in a single direction conferring tensile strength primarily in that direction. This can be seen in tendons and has been found in the STA (Marieb, 2009).
    ii. Dense irregular connective tissue has fibres arranged randomly in all directions and can be seen in the dermis (Marieb, 2009).

Collagen

Collagenic fibres found in connective tissue are found in large quantities in most sites in the body. They may occur as individual fibres or as large bundles of fibres clumped together to form structures of great tensile strength (Viguet-Carrin *et al.,* 2006; Bancroft & Gamble, 2008). Collagen in bone differs from other collagen found in the body, in that it becomes mineralized and is laid down in bands or lamellae roughly parallel to one another (Bancroft & Gamble, 2008). The organisation of collagen lamellae is responsible for the distinctive anatomical patterns of bone. This aspect of bone structure is controlled during bone formation to adapt the bone tissue to the stress experienced in a particular location (Viguet-Carrin *et al.,* 2006).

There are many types of collagen found in the body, however only collagen Type I and Type III will be discussed as these are speculated to be found in the tissue crossing the STA.

a. Collagen Type I forms the thick collagenous fibres forming the bulk of the body's collagen. The microscopic appearance of Type I collagen is bundles of tightly packed, thick fibrils (75nm diameter) with little interfibrillar substance (Ushiki, 1992).
b. Collagen Type III is only found in those tissues that also contain Type I collagen. Fibres known as reticular fibres contain collagen Type III. The reticular fibres containing collagen Type III range between 20 – 40nm in diameter and run singly or in small bundles (Ushiki, 1992).

1.4 Bone

Considering that the internal morphology of humeri is being investigated, bone structure and bone remodelling mechanisms are important to review as this may further the understanding of why the STA may develop.

1.4.1 Bone structure

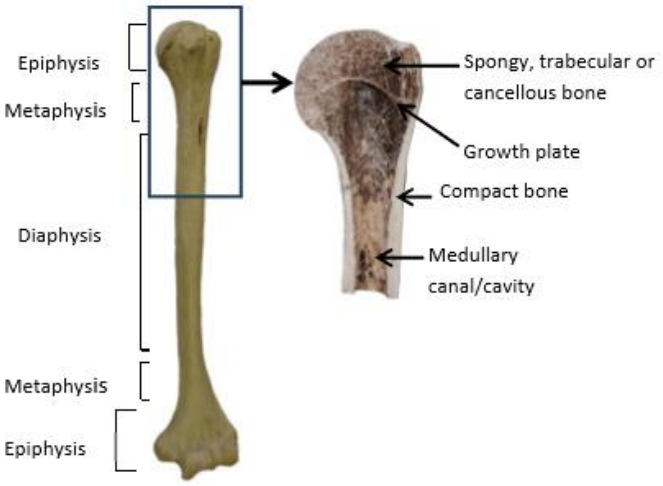


Figure 1.4: Humerus indicating different parts of the bone. Image courtesy of R Ndou.

Bone is a hard mineralized connective tissue consisting of organic and inorganic matrices. The organic matrix is mainly composed of collagen – primarily type I, with trace amounts of type III, IV and V – and ground substance which consists of H_2O, proteoglycans, glycosaminoglycans, osteonectins and osteocalcins. The inorganic matrix is made up of hydroxyapatite crystals and accounts for the majority of bone (Currey, 2002; Kramer & Allen, 2005).

The regular arrangement of collagen fibres and their ability to resist tension makes bone strong. This feature incorporates the function of bone, which is to provide support and protection of structures and organs in the body (Banse *et al.*, 2002; Viguet-Carrin *et al.*, 2006). Bone is a self-repairing tissue and is highly vascularised. Bone may be of two types, trabecular or compact/ cortical. Trabecular bone consists of thin anastomosing spicules known as trabeculae with interceding cavities that contain bone marrow. Trabecular bone is found in axial skeletal elements and the metaphyses and epiphyses of long bones, accounting for 20% of the human skeleton (Clarke, 2008). Trabecular bone consists of trabecular plates and rods which connect to form cavities that have a lattice-like appearance, this houses bone

marrow. This arrangement of trabecular bone makes it porous in nature. The bone marrow cavities are lined by connective tissue called endosteum – this layer contains osteoblasts and osteoclasts that are important in the bone remodelling cycle. Compact bone is made up of Haversian systems or osteons which are concentric lamellae of bone arranged around a central Haversian canal – this contains blood vessels, nerves and lymphatics & provides nutrients to the bone. Cortical bone consists of overlapping parallel osteons, which is a remnant of a completed remodelling cycle.

In long bones such as the humerus, the bone is composed of outer compact bone and inner trabecular bone (Drake *et al*., 2019). Structural stiffness and lightness of long bones are achieved by a medullary canal. Long bones grow in length by endochondral apposition on the endosteal surfaces and in width by the deposition of bone on the periosteal surface (Ruff & Hayes, 1988; Ammann & Rizzoli, 2003). Sex and population differences in the extent of periosteal apposition and endocortical resorption during growth and ageing lead to variations in the diameter and cortical thickness of bone and therefore the distance of cortical mass to the neutral axis of the bone, thus leading to the differences in bone strength (Ruff & Hayes, 1988; Duan *et al.,* 2005; Nieves *et al.,* 2005).

Bone fragility is more common in women than in men, partly because sex hormones in men do not rapidly decrease and there is no increase in bone remodelling rate in midlife (Schult *et al.,* 2004; Seeman & Delmas, 2006). Although perforation and loss of connectivity between trabeculae occur in men, bone loss in men proceeds more by trabecular thinning (due to reduced bone formation with each bone multicellular unit) than by trabecular perforation (due to increased bone resorption within each bone multicellular unit). Rapid remodelling does not slow down with age, it continues because of persistent hypogonadism in women, emerging hypogonadism in some men and secondary hyperthyroidism in both sexes (Schult *et al.,* 2004; Seeman & Delmas, 2006; Fonseca *et al.,* 2014). With continued remodelling, trabeculae perforate and some disappear completely. Remodelling is more active on the endocortical surface than on remaining trabecular surfaces. Cortical thinning and porosity reduces the resistance of bone to the propagation of cracks (Seeman & Delmas, 2006; Fonseca *et al.,* 2014).

Bone fabric is woven at sub-microscopic, microscopic & macroscopic levels. Optimal mass is adapted in size, shape and architecture for structural strength. Cortical bone consists of overlapping parallel osteons. A large number of osteons per unit of bone volume limits the

propagation of cracking because they obstruct the passage of a crack as it navigates between the many osteons. The entry of cracks into the osteon is blocked by the cement line delimiting each osteon and by concentric lamellae of mineralized collagen fibres that are packed in alternating loose and dense pattern & are orientated in various directions. Uncracked bone tissue within a crack forms a bridge that carries the load that would otherwise be used to drive the crack forward. Cracks are largely confined to older more densely mineralized interstitial bone between osteons (Qiu *et al.,* 2005). Although small confined cracks are undesirable they are a final means of dissipating energy as a defence against the alternative means of energy release imposed by the stress on the bone, fracture (Seeman & Delmas, 2006; Fonseca *et al.,* 2014).

Porosity in human bone varies from about 70 to 80% in cancellous bone sites and between 2 – 3% in cortical bone in young human adults. Cortical porosity may increase to 10 – 12% in disease states or some local regions of the skeleton. Porosity increases topographically from periosteal to endosteal and is greater near the endosteal surface because of higher remodelling rates. The gradient is more evident in bone from older people and/ or individuals with osteoporosis (Augat & Schorlemmer, 2006). Porosity is inversely and exponentially related to bone strength and modulus. A small increase in porosity can produce larger reductions of mechanical strength and stiffness (Augat & Schorlemmer, 2006; Sundh *et al,* 2017). Porosity is most easily measured microscopically in 2 dimensions from cross-sections of bone using stereological point cutting techniques (Thomsen *et al.,* 2005).

The presence of the STA is suggested to increase the risk of low energy fractures (Krishnamurthy *et al.,* 2011; Diwan *et al.,* 2013; Paraskevas *et al.,* 2012), therefore structural differences may be observed in humeri expressing the STA compared to humeri without the STA. There is a difference in the medullary canal dimensions of humeri with STA, such that a smaller medullary canal has been implicated with more gracile bones (Moores, 2006; Singhal & Rao, 2007; Paraskevas *et al.,* 2010; Krishnamurthy *et al.,* 2011). Ndou *et al.* (2015) found that humeri with STA have narrower medullary canals when factoring the size of the humeri. The differences in the volume, thickness and area of trabeculae and thickness of cortical bone in individuals with the STA have not been documented.

Robusticity refers to the strength of a bone as reflected by the shape and size (Stock & Shaw, 2007). The measurements taken for robusticity in the study conducted by Ndou & Schepartz (2016) for humeral shaft dimensions were found to be smaller in STA bearing humeri.

Robusticity was found to inversely correlate with STA formation. In all populations, it was found that females had a smaller shaft circumference with an increased presence of STA bearing humeri.

1.4.2 Bone remodelling

Cellular components & microscopic structure of bone

The mineral content in bone depends on the efficacy of the mineralization process, the mean bone age and size of the remodelling space. The main cells responsible for the bone remodelling cycle are osteoblasts and osteoclasts. Osteoblasts are responsible for the production of bone matrix and mineralization of bone (Kramer & Allan, 2005; Raggatt & Partridge, 2010; Crockett *et al.,* 2011; Parra-Torres *et al.,* 2013). They secrete collagen type I, osteopontin, osteocalcin and a ground substance constituting unmineralized bone known as osteoid (Kramer & Allan, 2005; Parra-Torres *et al.,* 2013). These cells are derived from osteoprogenitor cells that develop into osteocytes once the bone mineralises and entraps the osteoblast causing the osteoid to be released (Kramer & Allan, 2005). Osteocytes regulate calcium and phosphorus homeostasis under the influence of parathyroid hormone (PTH) and calcitonin (Crockett *et al.,* 2011; Parra-Torres *et al.,* 2013). Therefore osteocytes are responsible for the maintenance of the bone matrix (Kramer & Allan, 2005; Parra-Torres *et al.,* 2013). Osteoclasts are derived from monocytes and have a role in bone remodelling, specifically the breakdown and resorption of bone (Kramer & Allan, 2005; Raggatt & Partridge, 2010; Crockett *et al.,* 2011; Parra-Torres *et al.,* 2013).

Remodelling

Bone remodelling occurs through continuous cycles of bone resorption and formation to sustain skeletal integrity and biomechanical reliability (Raggatt & Partridge, 2010; Parra-Torres *et al.,* 2013), maintaining calcium homeostasis and optimum bone strength. The process is triggered by stress which causes micro-cracking and therefore removal and repair of this damaged area occur (Kramer & Allan, 2005; Raggatt & Partridge, 2010). Osteoclasts and osteoblasts are involved in the remodelling process (Fig. 1.5).

There are five stages of the bone remodelling cycle: activation, resorption, reversal, formation and quiescence however there is rarely a clear distinction between the phases (Raggatt & Partridge, 2010; Parra-Torres *et al.,* 2013). Additionally, the cycle is marked by cellular and molecular events

i) *Activation*: The bone remodelling cycle is caused by micro-damage to the bone (Raggatt & Partridge, 2010; Parra-Torres *et al.*, 2013). This micro-damage to the bone causes an interruption of normal vascular function and leads to activation of non-specific wound healing pathways. The cellular response during this stage is co-ordinated by and involves the secretion of a range of cytokines and growth factors that facilitate the recruitment of additional inflammatory cells in a positive feedback loop, as well as the migration of stem cells; these are implicated in bone formation (Schindeler *et al.*, 2008). In STA bearing bones this may be caused by the ulna and humerus articulation (Ndou, 2015).

ii) *Resorption*: Stress, which may be nutritional, hormonal or mechanical, leads to bone resorption (Hancox, 1972). Bone resorption is the breakdown of bone by osteoclasts, of which minerals are released into the bloodstream (Teitelbaum, 2000). Krishnamurthy *et al.* (2011) suggested that stress exerted on the humeral septum due to pressure from the ulnae processes during elbow motion may trigger resorption. Bone resorption occurs as a normal event (Hancox, 1972; Teitelbaum, 2000). Ndou & Schepartz (2016) suggested that resorption may be excessive in STA bearing humeri.

iii) *Reversal*: The bone begins the repair process during this stage. Macrophage-like cells deposits a binding layer to adjoin the newly deposited bone to the surface (Raggatt & Partridge, 2010; Parra-Torres *et al.*, 2013) Most fractures possess some level of mechanical instability & heal by bony callus formation. The stage is dominated by chondrocytes and fibroblasts which produce a semi-rigid soft callus that is able to provide support to the fracture as well as act as a template for the bony callus that will later supersede it at the beginning of the formation stage (Schindeler *et al.*, 2008). Ndou & Schepartz (2016) postulated that the repair process may be inadequate in STA bearing humeri.

iv) *Formation*: This is the most active stage of osteogenesis. During this stage, molecules are secreted which aid in bone formation. These molecules are secreted from osteoblast progenitors that have reverted to an osteoid and have differentiated. The molecules include Collagen type I, which is a principal organic component of bone and other non-collagenous proteins. Hydroxyapatite is incorporated into the new osteoid to complete the mineralization process (Raggatt & Partridge, 2010; Crockett *et al.*, 2011; Parra-Torres *et al.*, 2013). Vasculature is known to be critical for the formation of the hard callus, however, this is not the only determinant of fracture healing success. Ndou & Schepartz (2016) suggested that

bone formation in the septum may be inadequate due to the deficiency of hydroxyapatite in STA humeri.

v) *Quiescence*: The final stage of the remodelling cycle is characterised by the cessation of the cycle (Raggatt & Partridge, 2010; Parra-Torres *et al.*, 2013). Approximately equal amounts of resorbed bone would be replenished (Kramer & Allan, 2005). However abnormal remodelling occurs in various pathological diseases such as osteomyelitis and osteoporosis (Hancox, 1972).

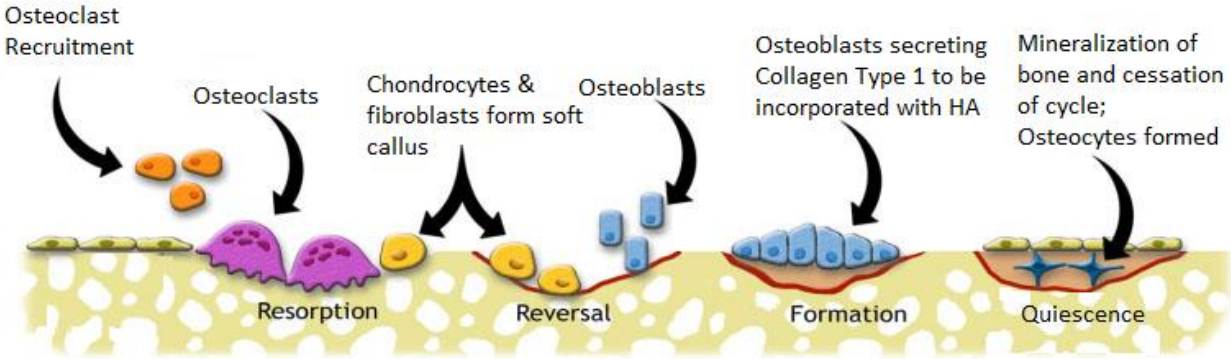


Figure 1.5: The bone remodelling cycle. Adapted from "Describe the process of bone remodelling" by OrthopaedicsOne https://www.orthopaedicsone.com/display/ Clerkship/Describe+ the+process+of+bone+remodeling

A negative balance in the bone multicellular unit compromises bone strength. When bone formation is less than the prior bone resorption, each remodelling event removes a small amount of bone from the skeleton resulting in bone loss and structural damage (Lorenzo, 2000). Furthermore, rapid remodelling is associated with an increased risk for fracture for several reasons. Firstly, during the resorption phase of remodelling more densely mineralized bone is removed and replaced with less densely mineralized bone, therefore, reducing bone stiffness and may lead to the bone cracking under usual loading conditions (Delmas, 2000; Boivin & Meunier, 2002). Secondly, resorption sites are temporarily unfilled thus creating stress concentrators that predispose a bone to micro-damage (Currey, 2002). Thirdly increased remodelling impairs incorporation of calcium hydroxyapatite and therefore impairs maturation of collagen, increasing the fragility of bone (Viguet-Carrin *et al.*, 2006). Consequently, the STA may be a result of this negative balance and the compensatory rapid remodelling and may increase the risk for future fractures in humeri with the STA.

Since remodelling occurs on bone surfaces, trabecular bone has more remodelling sites per unit volume compared to cortical bone. A greater proportion of trabecular bone is turned over and lost if there is a negative balance (Parfitt *et al.*, 1983). The high remodelling rate and resorption cavities produce a loss of trabecular plates and decrease the density of the trabecular bone and therefore decreases the overall bone strength (Parfitt *et al.*, 1983; van der Linden *et al*, 2001).

1.4.3 Bone mineral density

Bone is composed of collagen type I which is stiffened by crystals of calcium hydroxyapatite. An increase in bone mineral density (BMD), as well as tissue mineral density, increases stiffness at the expense of flexibility, therefore variations in these mineral densities affect function. There are observed differences in bone mineral content as well as mineralization rate with regards to age, sex and ethnicity. Males exhibit an increase in bone density with age to a greater extent than females. Females exhibit changes in bone mineral content and bone mineral properties during pregnancy and lactation. This may be due to the correlation with the hypoestrogenic condition but have an impact on the fragility of bone. In addition to this, malnutrition causes decreased bone mineral density and bone mineral content as it causes a change in bone mineral composition and bone mineral crystal size (Kim & Kim, 2003; Seeman & Delmas, 2006; Yao *et al.*, 2013).

A deficiency of magnesium increases bone remodelling. Therefore, the smallest most soluble bone crystals are lost to provide the body's needed magnesium ions. Bones with larger mineral crystals than those of magnesium have a magnesium excess and therefore a decrease in mineral formation and an increase in crystal size of existing mineral (Castiglioni *et al.*, 2013). Vitamin D deficiency (or alterations in body calcium and phosphate stores that are dependent on vitamin D) shows a decrease in mineral content and a decrease in mineral crystal size. Bones of animals with vitamin D deficient osteomalacia, in general, are more brittle than those of age, sex and/ or sized matched controls indicating the importance of mineral size and content on bone properties (Lieben & Carmeliet, 2013; van Driel & van Leeuwen, 2017).

A deficiency in vitamin B_6 leads to diminished elastic properties of bone due to the alterations in the collagen structure. Collagen is important for bone mineral deposition as the cross-links between and among collagen molecules appear to be related to mineralization. Whereby the cross-linking pattern in mineralized bone is different from that in non-

mineralized bone. Collagen limits the extent to which minerals can aggregate and the length to which they can grow. Bone adaptation may induce mineral deposition (Donnelly *et al.*, 2010; Nair *et al.*, 2013).

The volume of cortical bone compared to the volume of trabecular bone (Kimura *et al.*, 2012), as well as the increased porosity of the bone, may influence bone mineral density (BMD) (Oei *et al.*, 2013; Leidig-Bruckner *et al.*, 2014). Additionally, females have a lower BMD than males and are therefore more susceptible to osteoporosis and fractures (Oei *et al.*, 2013). This may be due to the increased number of Haversian canals in females, which increases porosity and decreases bone mass (Thompson, 1980). STA bearing humeri have an increased risk of fracture (Krishnamurthy *et al.*, 2011; Diwan *et al.*, 2013; Paraskevas *et al.*, 2012), therefore BMD is expected to be lower in STA bearing humeri compared to humeri without the STA. Establishing differences in BMD by STA status will contribute to our existing knowledge of STA expression.

1.4.4. Biomechanics of bone

The strength of bone is determined by its material composition and structure (Currey, 2002). Bone should ideally be stiff and able to resist deformation for loading to occur. Further, bone should be flexible to absorb energy by deforming and resist compressive & tensile forces acting on the bone without cracking. If bone is brittle, the energy imposed during loading will be released by structural failure resulting in initial micro-cracking and then a complete fracture, however, if bone is too flexible and deforms beyond its peak strain it will also crack. Regardless, bone is able to find a balance between these contradictory needs (Wainwright *et al.*, 1982; Ammann & Rizzoli, 2003) In terms of fracture risk, decreasing bone mineral leads to an exponential increase in fracture risk. Additionally, bone architecture has a great influence on bone strength and the risk of fracture and may be influential on STA formation (Jiang *et al.*, 2005).

Wolff's law and Young's modulus

According to Wolff's Law, organisms are able to adapt their structure to changing environmental conditions; similarly bone has the ability to respond to localized mechanical strain. Low levels of strain result in bone resorption which in turn leads to more strain. The humerus is subjected to low levels of strain during daily activities resulting in bone resorption (Ruff *et al.*, 2006). However, the STA may be resultant from higher levels of continuous strain.

Similarly, Young's modulus is the measure of the ability of a material to withstand changes in length when under lengthwise tension or compression, materials with a low Young's modulus do not withstand strain as well as those with higher Young's modulus values. In bone Young's modulus ranges between 10 – 25 GPa from trabecular to cortical bone, whereby most changes in bone caused by stress and subsequent remodelling can be seen clearly in trabecular bone and to some degree in cortical bone (Rho *et al.,* 1993).

Mechanics of materials

Bones are physical objects that obey the laws of mechanics. The primary laws that concern deformable objects like bone are Newton's three laws of motion and Hooke's law of elasticity of solid material. Hooke's law states that there is a linear relationship between the force and the deformation of a solid object. Both Newton's laws and Hooke's law form the foundation of the mechanics of elastic objects. The mechanical behaviour of bone in normal physiological situations is similar to the mechanical behaviour of an elastic object (Lu & Chang, 2012; Lefèvre *et al.,* 2015).

Collagen orientation

As previously mentioned, collagen fibres play a significant role in bone remodelling and STA formation, therefore the collagen fibre orientation may be integral in STA aetiology. There is an association between mode of strain and collagen fibre orientation. Osteons with longitudinally orientated collagen fibres were stronger and stiffer in tension than osteons with collagen fibres orientated transversely. Conversely, osteons with transversely orientated collagen fibres were stronger and stiffer in compression than those with longitudinally orientated fibres (Riggs *et al.,* 1993; Bakbak *et al.,* 2011).

1.5 Bone imaging modalities

As bone imaging modalities were used in the investigation of the STA, it is important to understand the mechanisms of how different modalities work. Bone imaging modalities employ two general measures for assessing bone health, namely bone mass and bone quality. Bone mass is the measure of the number of minerals contained in a certain volume of bone. It is, therefore, the measure of BMD and is the standard measure of bone health (Compston, 2006). The imaging modalities used in the evaluation of bone health are set up to respond to either BMD or bone quality. BMD accounts for only part of the variation seen in bone strength and only some of the observed reduction in fracture risk that occurs with treatment. Therefore, evaluation of bone quality encompasses the measurement of bone structure and quality of trabecular and cortical bone as well as bone mass, providing a better prediction of fracture risk (Griffith & Genant, 2011).

1.5.1 Imaging modalities used for the evaluation of bone mineral density

Dual X-ray absorptiometry

Dual X-ray absorptiometry (DXA) is the most readily available surrogate marker of bone strength and fracture risk (Griffith & Genant, 2011). A composite image is created by two x-ray beams, one emitting low energy radiation and one emitting high energy radiation. The BMD is evaluated in a two-dimensional plane (mg/cm^2) (Bauer & Link, 2009). The depth is not taken into consideration (Griffith & Genant, 2011). DXA is limited in that it is a composite measure of both the cortical and trabecular bone and is therefore prone to overestimation of BMD from degenerative-type hyperostosis. However, DXA is advantageous in a clinical setting as it administers relatively low radiation compared to other imaging modalities (Griffith & Genant, 2011).

Quantitative computed tomography

Quantitative Computed Tomography (QCT) is derived from computed tomography in that it employs a detector to capture electrons from an x-ray beam. These electrons are either absorbed or pass through the specimen depending on its density, providing the volumetric information about the tissue. QCT is able to detect changes in the more metabolically active making it a more sensitive discriminator of BMD changes regarding cortical and trabecular bone information than DXA, however, it administers higher levels of radiation (Griffith & Genant, 2011).

1.5.2 Imaging modalities used for the evaluation of bone quality

Radiography

This technique utilises basic x-ray technology and is a readily available technique with a high spatial resolution capable of providing fine bone detail. However, individual trabeculae cannot be visualized and it is dependent on the depth of tissue under investigation (Griffith & Genant, 2011).

Magnetic resonance imaging

Magnetic resonance imaging (MRI) is unique in that it employs magnetic fields in the analysis of tissues as opposed to ionized radiation. The magnetic field is directed towards the nuclei of hydrogen atoms in the water content of tissue (Griffith & Genant, 2011). Although MRI provides greater contrast for soft tissue than other radiological techniques, bone is a poor respondent to the technique due to the low water content. Trabecular bone is visualized as dark spaces or artefact gaps around the bright bone marrow, which has high water content (Bolliger *et al.,* 2008; Griffith & Genant, 2011). MRI is favourable as it has no exposure to ionizing radiation, however, it is disadvantageous in that it has a long scanning time to achieve high spatial resolution for trabecular bone (Griffith & Genant, 2011).

Micro-CT

Micro-CT (µCT) uses x-ray attenuation data acquired at multiple viewing angles to produce a three-dimensional (3D) reconstruction of the specimen that characterized the spatial distribution of material density (Bouxsein *et al.,* 2010). µCT scans may be used to provide an estimate of bone tissue mineralization by comparing x-ray attenuation in the bone with that of hydroxyapatite standards. This voxel-based mineral density data along with high-resolution morphology of the bone determined from the µCT scan can be used to create µ-finite element models to estimate mechanical behaviour (Jiang *et al.,* 2005).

The advantages of µCT for assessment of bone mass and morphology in excised specimens, such as those used in this study, include a significantly larger volume of interest is analysed when compared with 2D histology. Moreover, this technique allows for direct 3D measurement of trabecular morphology, rather than inferring values based on stereological models as is done with standard histologic evaluations. Lastly, it allows for an in-depth investigation of bone morphology in a non-destructive manner (Jiang *et al.,* 2005; Bouxsein, *et al.,* 2010). Therefore µCT was chosen as a suitable technique for the present study.

µCT measures overestimate trabecular thickness relative to histomorphometric measures. This may be attributable to inadequate resolution of µCT images relative to the trabecular size, the use of a plate model to estimate trabecular thickness in 2D histomorphometry versus direct 3D methods in µCT, poor threshold selection, and/or the fact that 3D µCT measurements of trabecular thickness include trabecular intersections (nodes), which increases thickness values compared with measurements made only on trabecular struts (Chappard *et al.,* 2005). However, a high correlation between the two techniques provides a strong rationale for the use of µCT to assess skeletal morphometry (Chappard *et al.,* 2005; Bouxsein *et al.,* 2010).

1.6 Clinical significance of the STA

Knowledge of the presence of the STA may aid in surgical corrections (Singhal & Rao, 2007; Paraskevas *et al.,* 2010; Krishnamurthy *et al.,* 2011). For example, an intramedullary fixation may be used in corrective surgery of a humeral fracture. This procedure entails the insertion of a nail or rod into the vertical length of the medullary canal, which is then fixed to the humerus so as to stabilise the fracture (Moores, 2006). The difference in the medullary canal dimensions in individuals with the STA, such that the medullary canal is shorter and narrower, may lead to difficulties in the corrective surgery and may increase the risk of future fractures if an incorrect rod or nail is chosen (Singhal & Rao, 2007).

1.7 Research questions

Although research into the prevalence and the aetiology of the STA has been conducted, the internal structural morphology of humeri with the STA has not been described. How do humeri bearing the STA differ from humeri without the STA with regards to internal bone morphology? Secondly, what is the histological composition of the STA region, and how can this be interpreted in terms of STA formation?

1.8 Aim

This study aimed to investigate the differences in the internal bone morphology in individuals with and without the STA to understand how variation in bone morphology is related to STA status.

1.9 Objectives

1. To assess the trabecular morphological parameters of humeri with and without the STA by comparing the thickness, number and size of trabeculae and volume of trabecular bone in the proximal and distal epiphysis of using µCT techniques.

   Hypothesis: Trabecular morphological parameters are poor in STA bones.

2. To investigate, using histological techniques, the theory (mechanical) that the bony septal plate between the olecranon and coronoid fossae is resorbed primarily from the posterior aspect in STA formation due to impingement by the ulnar olecranon process.

   Hypothesis: The posterior plate will be resorbed if the ulnar olecranon process is implicated in STA formation.

3. To determine the composition of the dense regular connective tissue crossing the STA, by histological processes.

   Hypothesis: Collagen type I and type III will be present

Chapter 2

Materials and methods

In order to achieve the aims and objectives outlined in Chapter 1, two separate studies were undertaken:

i. Histological techniques were employed to investigate the microstructure and composition of the tissues in the STA region from cadavers.
ii. Micro-CT (μCT) scans of dry bones were used to evaluate bone trabecular structure in humeri with and without STA.

2.1 Cadaveric histological tissue analysis

2.1.1 Sample

Tissue samples were obtained from 21 individuals (15 females and 6 males) in the Teaching Cadaver Collection of the University of the Witwatersrand. Due to the variations in laterality of the STA occurrence, 30 samples were collected as outlined in Table 2.1. It was not possible to differentiate between humeri with and those without the STA by visual examination of the septum between the coronoid and olecranon fossae (where the STA is located). Through visual examination, the septum appeared opaque in some humeri and translucent in others. Humeri with an opaque septum were definitely without the STA as light could not pass through the septum. Translucent septa could either be with or without the STA. Therefore, two control groups were established, involving 10 samples with an opaque septum and 10 samples as translucent septum controls. Use of X-ray determined the classification of the translucent septa as either having or not having the STA. On X-ray examination, samples with an opaque septum had trabecular throughout the septum, these were classified as opaque controls. Those with translucent septa were characterised by trabecular exhibiting a gradient transition to the centre. These controls were used for the tissue resorption analysis (as in objective 2). The remaining 10 samples were those with the STA present, characterised by an abrupt change of trabecular bordering the central area of no trabeculae (the STA) with a clearly defined bony border on radiographic assessment.

Table 2.1: Cadaveric samples. The number of individuals assessed and the distribution of the observed characteristics, which are represented on the left or right sides or bilaterally. The last column represents the total number of samples collected.

		Individuals assessed		Distribution of the observed characteristic			Number of samples
Group		**Sex**		**Left**	**Right**	**Bilateral**	**Total**
Controls	**Opaque**	Female	4	1	1	2 (4)	10
		Male	3	2	0	1 (2)	
	Translucent	Female	5	2	0	3 (6)	10
		Male	1	0	0	1 (2)	
STA present		Female	6	2	3	1 (2)	10
		Male	2	0	1	1 (2)	
Total			21	7	5	18	30

2.1.2 Dissection techniques for tissue collection

With the body in the supine position, an incision was made on the lateral aspect of the arm from the shoulder joint to the wrist joint. A transverse incision was then made at the wrist joint and the skin was reflected medially. Once the subcutaneous fat and overlying fascia were cleared, the bicipital aponeurosis was cut and the biceps brachii was reflected superiorly. Brachialis and coracobrachialis were reflected laterally. The brachioradialis was then separated from the flexors to ensure the anterior surface of the distal humerus was not obstructed by any tissue. The brachial artery, basilic and cephalic veins, as well as the median and ulnar nerves, were kept intact and displaced laterally and medially using straight teasing needles (Fig. 2.1).

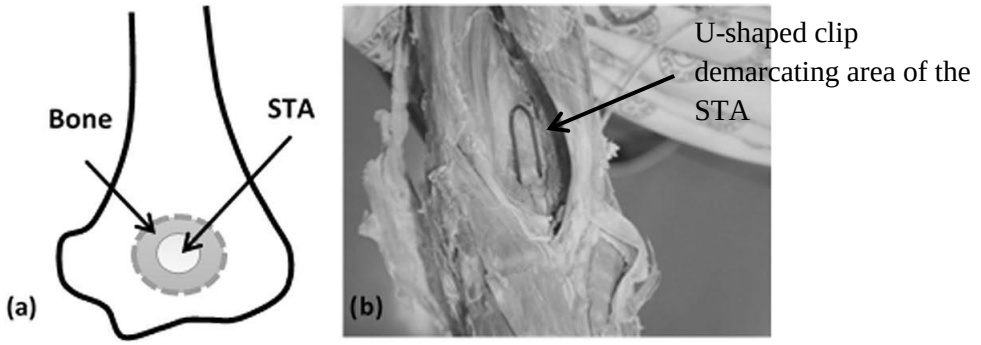


Figure 2.1: Dissection of the elbow joint in preparation for tissue harvesting

To expose the posterior surface of the humerus, the elbow joint was flexed to ensure the olecranon process did not obstruct the olecranon fossa. A transverse incision was then made to separate the triceps brachii from its distal attachment on the olecranon fossa. Oblique incisions, two proximally and two distally, were made on either side of the transverse incision to create pockets for the X-ray sensor placement.

Identification of the STA

As the physical observation of the STA is not generally possible in cadaveric specimens, a portable dental X-ray machine (ARIBEX NOMAD® CE eXaminer) was used (Fig 2.2.). The method described by Ndou *et al.* (2018) takes the following into consideration: (i) the optimal distance from the X-ray machine barrel to the subject, (ii) the stability of the X-ray machine and (iii) establishing the correct exposure to determine humeri with and without the STA. As the septum is thin, high exposure may lead to a false positive. Additionally, the duration of X-ray exposure affects the image produced as overexposure may also lead to a false positive.

The standardized distance was determined as 33 cm. In order to stabilize the X-ray machine and maintain the standardized distance, a special wooden table was constructed (Fig. 2.2, Ndou, 2018). The humeri were exposed to 40kV and then 35kV to confirm the image produced. The exposure lasted for approximately three seconds.

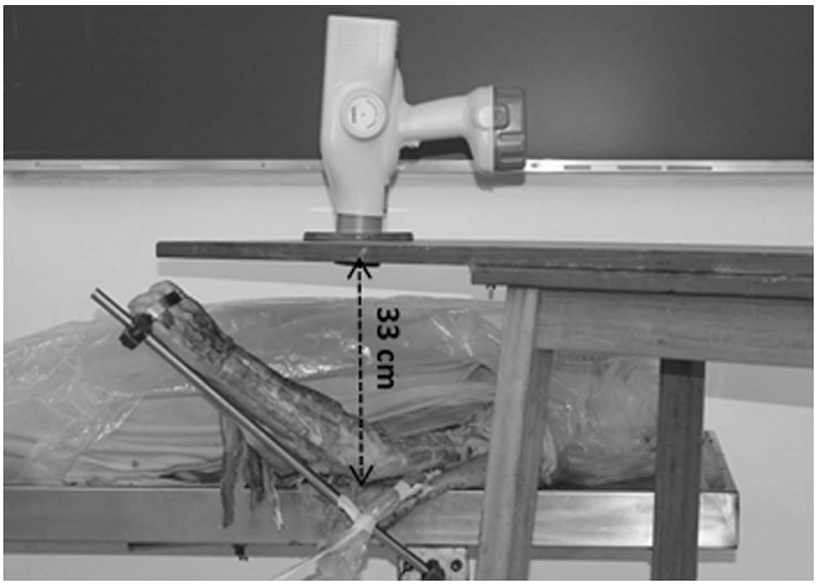


Figure 2.2: Portable dental X-ray machine positioned in the custom-designed table

During the scan, the elbow was flexed at 135°-140°, as measured using a goniometer, to displace the olecranon process from the olecranon fossa (Fig. 2.2). The sensor was then placed directly beneath the olecranon fossa on the posterior aspect of the bone. The size of the sensor (35 mm X 27 mm) allowed for the entire olecranon fossa to be in view.

The STA was considered to be present when a clear boundary, surrounded a radiolucent area devoid of trabecular bone was observed (Fig. 2.3A). Specimens were categorized as 'intermediate' when a boundary could be seen but the area it surrounded appeared hazy. Alternatively, 'intermediate' referred to cases in which the boundary was unclear but a distinct radiolucent area was visible (Fig. 2.3B). These made up the control samples with a translucent septum. In contrast, the STA was considered to be absent when the entire septum appeared radiopaque and exhibited trabecular bone throughout (Fig. 2.3C).

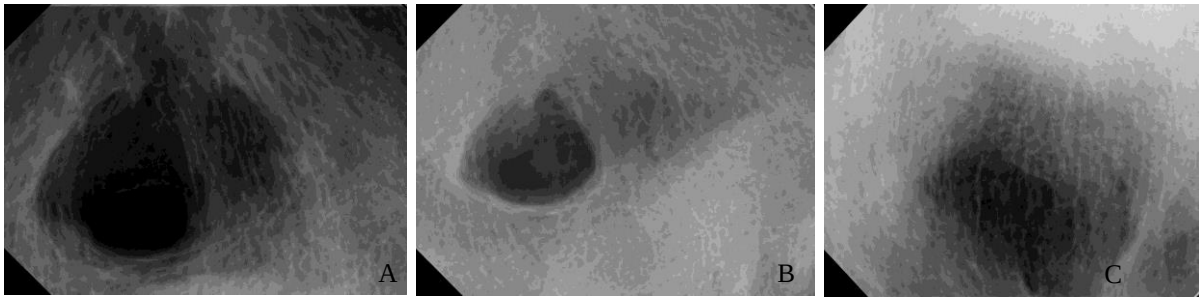


Figure 2.3: X-rays of the humerus indicating (A) STA presence, (B) a translucent septum and (C) an opaque septum (STA absent) (C)

Tissue harvesting

When the STA or an intermediate control was observed on the X-ray, a U-shaped metal clip was used to demarcate and enclose either side of the STA. This was then radiographed to identify and mark the boundaries of the STA using a marker (Fig. 2.4).

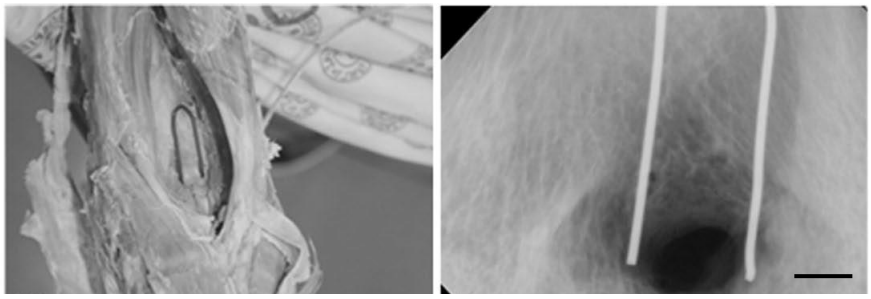


Figure 2.4: U-shaped metal clip demarcating the STA boundaries in a cadaver and on a radiograph

A 17mm hole saw was used to harvest the tissue as this diameter ensured the STA and surrounding bone was included. The marked boundaries were used to guide the saw so to avoid cutting through the area of the STA. The harvested tissue was then radiographed with a thin wire to indicate where the tissue would be bisected following decalcification (Fig. 2.5). Bisection of the tissue was done to ensure that the area of the STA is represented within each cut section on the microtome. Tissue samples were stored in fresh 10% neutral buffered formalin (Appendix B). 10% neutral buffered formalin was chosen as it has little to no effect on the tissue samples.

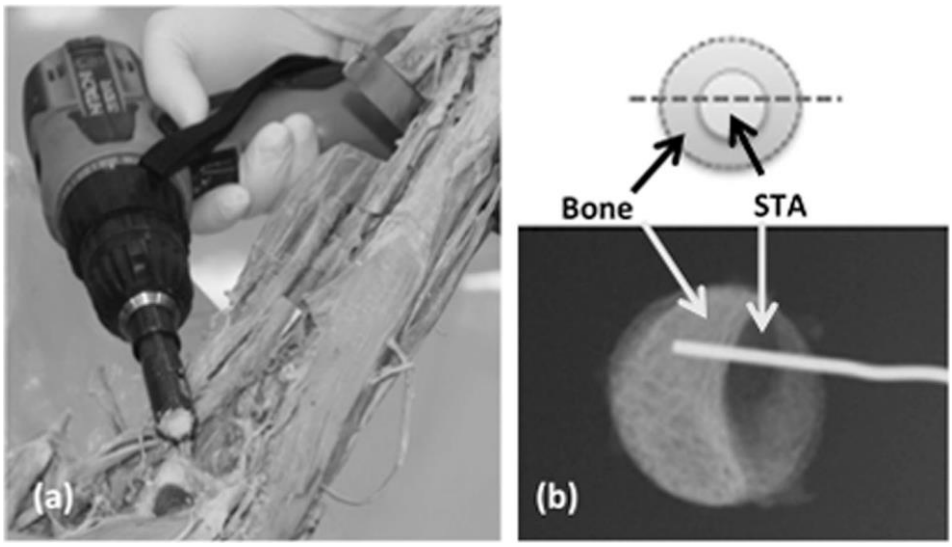


Figure 2.5: Thin wire indicating the point of bisection to ensure the area of the STA was represented when cutting sections on the microtome

Bone decalcification

The samples were rinsed in distilled water to remove excess formalin and decalcified for three weeks before being processed for histological assessment. Decalcification is a process in which calcium ions are removed to make the bone softer and to enable sectioning of the tissue. A 10% solution of formic acid (Appendix C) was considered to be the ideal agent for decalcification as it is a gentler decalcifying agent for smaller bone pieces (Alers, 1999; Shibata *et al.*, 2000; Bancroft & Gamble, 2008).

To test for the endpoint of decalcification, approximately 2ml of formic acid in which the sample was immersed was drawn and placed in a separate test tube, 5ml of ammonium oxalate was then added to that same tube and left to stand for 30 minutes to observe for

precipitate. The absence of precipitate indicated complete decalcification of the bone sample. All samples were rinsed in running tap water for 30 minutes and placed in 10% neutral buffered formalin in preparation for tissue processing.

Tissue processing

Following decalcification, the tissue was bisected with a scalpel and the posterior surface was marked with Pelikan India ink. An automatic processor (Shandon Citadel 1000) was used to take the tissue through different grades of alcohol before embedding the tissue in wax (Appendix D).

Paraffin wax embedding

An embedding table was used to embed samples in paraffin wax. The embedding wax, forceps and moulds were preheated to 60°C before the embedding process. Tissue samples were positioned in the metal moulds, filled with molten wax and covered with plastic cassettes. To ensure the samples were identically embedded, the cassettes were placed with the labelled section close to the posterior surface of the sample. The wax blocks were then allowed to cool on a frosted surface before they were removed from their moulds.

Microtome sectioning

Excess wax surrounding the block was trimmed with a blade. The blocks were cut to the level of the tissue with the microtome. Blocks were cooled on ice before cross-sections (5µm thick) were cut. To flatten the tissue sections, each section was floated in 30% ethanol and subsequently placed in a preheated water bath at 45°C. Once the sections were flattened in the water bath, forceps were used to separate the sections. Individual sections were then mounted onto silane coated microscope glass slides (Fig. 2.6).

Sections were separated and stained with haemotoxylin & eosin (H & E) for morphological assessment of the bone (Appendix E), a Rapid One-Step Mallory-Heidenhain Stain (Appendix F) was done for connective tissue identification (Cason, 1950) and a picrosirius red stain allowed for the distribution of collagen type I and type III to be identified (Appendix G). These analyses aid in understanding the formation of the STA with regards to the resorption of bone in the bone remodelling process.

H & E	Rapid One Step	Picrosirius red	Extra slide	Extra slide	Picrosirius red

Figure 2.6: Sequence of stains of the sections. Two extra slides were allocated for additional stains if necessary.

2.1.3 Staining of sections

Haematoxylin and eosin staining

The Haematoxylin and Eosin stain is used to determine the morphology of the tissue. Haemotoxylin stains the tissue blue/ basophilic, while eosin stains the connective tissue pink/ eosinophilic. Sections were dewaxed in xylene for 10 minutes and a fresh container of xylene for 5 minutes and rehydrated by passing them through a series of alcohol concentrations for 30 seconds each and rinsed in running tap water for 5 minutes. The sections were then stained in haematoxylin for 20 minutes, washed in running tap water for 5 minutes, differentiated in periodic acid for 1 dip, rinsed in tap water for 5 minutes. Sections were counter-stained in Eosin for 10 minutes and briefly rinsed in running tap water for 2 minutes. Sections were then dehydrated by passing them through a series of increasing alcohol concentration for 2 minutes each, cleared in 2 changes of xylene for 10 minutes each and mounted with Entellen (Appendix E)

Rapid one-step mallory-heidenhain staining

The rapid one step mallory heidenhain stain is used to identify connective tissue. The results of this stain on tissue are blue for collagen, shades of blue for ground substance of cartilage and bone as well as other hyaline substances. Nuclei stained red, while erythrocytes and myelin stain yellow. Elastin was found to stain pale pink or sometimes yellow.

Sections were dewaxed in xylene for 10 minutes and a fresh container of xylene for 5 minutes and rehydrated by passing them through a series of alcohol concentrations for 30 seconds each and rinsed in running tap water for 5 minutes. The sections were then stained in the working solution for 20 minutes and washed in running tap water for 1 minute. Sections were then dehydrated in 2 washes of Absolute Alcohol for 30 seconds, rapidly cleared in 2 changes of xylene then left to blot overnight. Sections were then mounted with Entellen the next day (Appendix F)

Picrosirius red staining

Collagen Type I presence is integral in the bone remodelling cycle, and collagen as a whole is vital in maintaining the structural integrity of the tissue that it is found in (Role of Collagen, pp 6). As such the Pirosirius red stain, in conjunction with viewing the sections under polarised light, was chosen to detect quantify and analyse the collagen found in the bone sections. As previously stated Collagen Type I is important in bone remodelling as it aids bone formation. Similarly, Collagen Type III is generally found in connective tissue and bone and may, therefore, be found in the tissue crossing the STA.

The outcome of this stain is shown in five fundamental colours, which are attributed to different structures. Under polarized light, larger collagen structures appear bright yellow or orange; retic fibres and thinner collagen fibres appear green; sulfated mucopolysaccharides are stained in violet; red blood cells stain in pale yellow and muscles stain in pale orange. Sections were dewaxed in two changes of xylene for 5 minutes each and then rehydrated in two changes of 100% alcohol and one change of 95% alcohol for 5 minutes each. The slides were then washed in running water for 5 minutes and pre-treated in 6% Nitric Acid for 5 minutes. The sections were then stained in Toluidine Blue for 10 minutes and washed in distilled water for 10 seconds until the toluidine blue was washed out. The sections were then stained in picrosirius red for 5 minutes and washed in distilled water for 10 seconds until the excess picrosirius was removed. Sections were then left to blot dry at room temperature for 1 hour before passing through one change of 95% alcohol and two changes of 100% alcohol for 5 minutes each so that they would be dehydrated before passing through two changes of xylene. Eventually, the sections were mounted using Entellen (Appendix G).

2.1.4 Imaging of sections

Images of the sections were captured using the Olympus BX63 Fluorescence Microscope, housed in the Microscopy and Microanalysis Unit, University of the Witwatersrand. Analysis

of these sections was conducted using Fiji ImageJ software. An overview of the entire section was obtained using a 4x objective lens and the stage navigator function on Olympus CellSens™ software, allowing for measurements to be taken on the whole section. The 10x objective lens was used to obtain images used for qualitative purposes. All images were taken with the brightfield observation method. As the samples were anisotropic, Z-stacking was done to obtain a sharper image.

2.1.5 Measurements for the resorption of bone

The degree of resorption on the anterior and posterior plates of bone in the region of the STA was determined through a series of quantitative measurements, as depicted in Figure 2.7. For each section, a length measurement of the entire section was taken; subsequently, width measurements were taken at three positions: the 25^{th} percentile mark, the 50^{th} percentile mark and the 75^{th} percentile mark. Similarly, three width measurements for the entire distance of the STA were obtained at the previously mentioned marks once the region of the STA was determined.

For the control group with a translucent septum, width measurements at the previously indicated percentiles were taken for the anterior and posterior plates (Fig. 2.7C). Finally, the area of the entire STA, including the plates for the control group with a translucent septum, was attained (Fig 2.7A, C). For the control group with an opaque septum, the measurements of the distance of the "STA" were not possible (Fig. 2.7B).

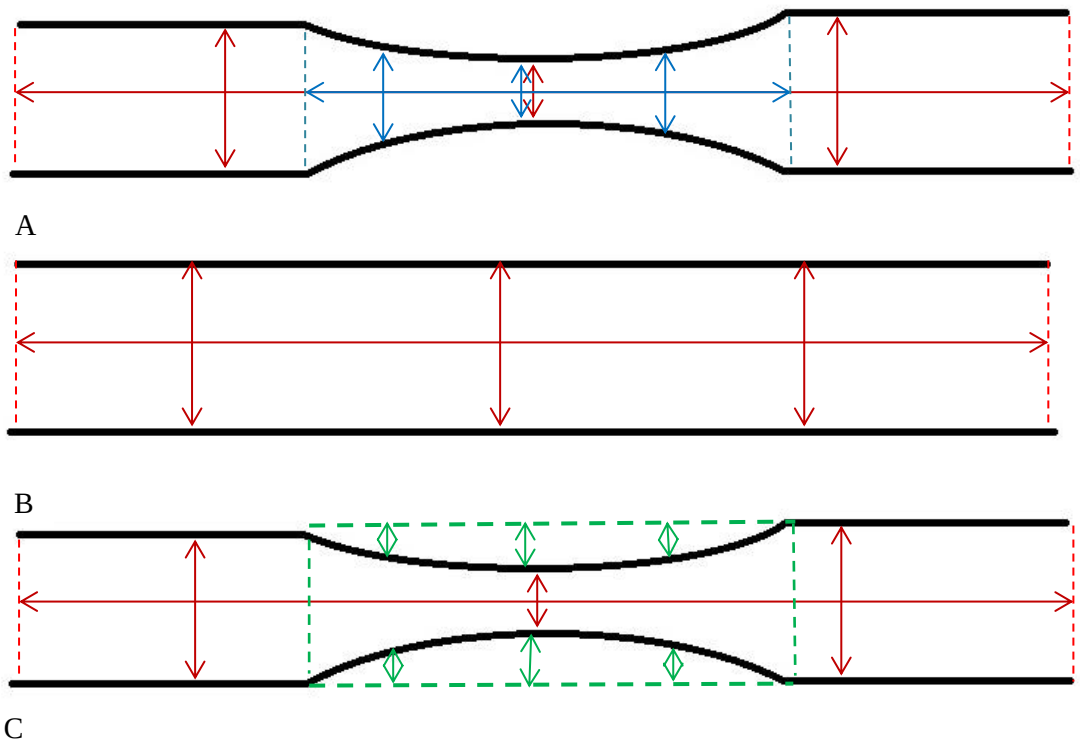


Figure 2.7: Diagram of the measurements taken from bone sections with (A) the STA (B), the control group with an opaque septum and (C) the control group with a translucent septum

The Picrosirius red stained sections were used to measure the density of the bone, as compared to connective tissue, on the overall bone as well as a comparison of anterior and posterior surfaces in the control group with a translucent septum. These results were obtained by measuring the area of bone, without the area occupied by trabecular space, and the area of connective tissue. These measurements were duplicated on the second set of Picrosirius red stains to ensure the accuracy of measurements.

2.1.6 Measurements of bone area: anterior vs. posterior

The comparison of bone area from the anterior aspect of the bone to the posterior aspect of the bone was measured as a gradient. To do this, a standard length of 8 mm was established per section and multiple rectangular areas were plotted to include the most anterior and most posterior portions of bone in these rectangular plots. Each rectangular plot was further divided into five equal squares creating a gradient from anterior to posterior (Appendix H). The area within each square was then measured and the squares were compared to identify whether there was a difference in bone densities on the anterior aspect compared to the posterior aspect (Fig 2.8).

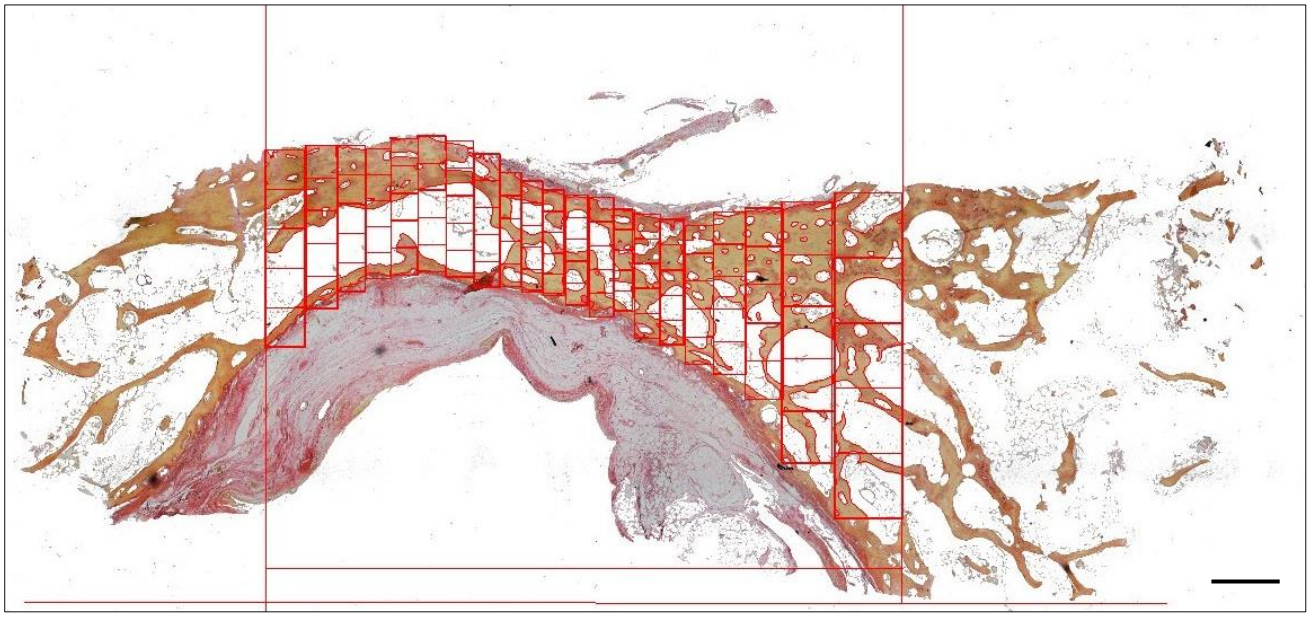


Figure 2.8: Area measurements taken to compare the bone area on the anterior and posterior aspects of the bone section

2.2 Micro-CT bone structural analysis

2.2.1 Sample of dry bone specimens

Thirty paired humeri were selected from the Raymond A. Dart Collection of Human Skeletons housed at the University of the Witwatersrand. These humeri belonged to females of African descent between the ages of 18 and 50 years. They were chosen to represent the subpopulation in South Africa with the highest frequency of STA bearing humeri (Ndou, 2015). These humeri included 15 pairs with the bilateral presence of the STA and 15 pairs with bilateral STA absence to control for side differences. The bones were free of any visible pathologies. The sample of 30 females is considered to be large enough to represent a normal

distribution (Hogg & Tanis, 2001). The age range was set so as to include individuals with fused epiphyses as well as to minimize the effects of senescence on the humeri.

2.2.2 Micro CT methods

Measurements of the internal structure of the humerus

µCT scans of the bones were taken at the Evolutionary Studies Institute, Paleosciences Centre, Microfocus X-ray Computed Tomography (CT) Facility of the University of the Witwatersrand using a Nikon XTH 225/320 LC dual-source industrial CT scanner (Table 2.2). The scans allowed for an examination of the internal structure of the bone. The trabecular bone volume, trabecular quantitative measures (the thickness, size and number of trabeculae) and the cortical thickness and medullary canal width were determined for the measurement of bone mineral density (BMD) as described in Table 2.3.

Table 2.2: Parameters for the µCT scans

Variable	Description	Measurement
Voxel size	Three dimensions defining the discrete unit of the µCT image	$40\mu m^3$
X-ray energy	Energy proportional to the frequency of X-ray photons	70kV
X-ray intensity	X-ray tube current	95µA
Frame averaging	Number of repeated measurements at each tomography projection	1
Projections	Number of tomographic viewpoints used for reconstruction	1000
Tomographic rotation		360 degrees
Scanning time		16 minutes

A CT works on the same principles as an x-ray machine, whereby x-ray photons are emitted through the body and the machine detects the number of rays that are able to penetrate through to the other side. Thousands of data points are taken to create three-dimensional slices of the specimen (Brenner & Hall, 2007; Retsky, 2008). In µCT, the same method is used but on a smaller scale with an increased resolution. It allows for the representation of 3D microscopy without the destruction of the sample. This is done through a micro-focus x-ray source, which illuminates the object, and a planar x-ray detector, which collects the magnified projection images. A computer is then able to synthesize a stack of 2D virtual cross-section slices through the object while the image rotates to produce a 3D representation of the scanned bone (Bouxsein *et al.*, 2010).

Reconstruction of the slices to create a 3D image

CT reconstruction is the process in which 2D projections, captured whilst rotating the sample, are used to produce a 3D volume file. The method used for reconstruction of the scans is known as a filtered back-projection (Kak & Slaney, 1999; Kumar & Hans, 2016). This can only be used for 2D parallel beam projecting geometrics and involves two phases (back-projection and filtering), although these occur simultaneously.

1. *Back-projection:* Each point of the object domain receives a value of the detector point where it projects to. The detector point is then "smeared" out on the object domain. This is done over all the projection angles. The values of each projection angle are then summed up. As more angles are back-projected the image becomes clearer, however, it does not become sharp and focussed (Kak & Slaney, 1999; Kumar & Hans, 2016). This is due to the severe under-representation of high frequencies in image processing. Whereby, low frequencies depict smooth surfaces and high frequencies depict details and sharp edges, therefore most images are not sharp, however, the second phase of the method corrects for this misrepresentation (Kak & Slaney, 1999).
2. *Filtering:* A high pass filter on the detector function (which allocates detector points), suppresses low frequencies therefore the resulting image is not overly blurred. The filter that is applied undergoes certain mathematical transformations to narrow down the frequencies. This results in a spectrum allowing for high frequencies to be given importance and low frequencies to be suppressed. There is a cutoff, and all frequencies higher than that are set to 0 in order to reduce noise in the reconstructed image. After filtering, the spectrum is inversed resulting in a new detector function which is then back-projected over the object domain (Kak & Slaney, 1999; Kumar & Hans, 2016).

All scans were reconstructed using the software package CT-Pro 3D from the Nikon Metrology XT software suite version 2.2 and stored for analysis as described below.

2.2.4 Trabeculae morphological parameters

The following measurements were conducted to assess the bone trabecular morphology. These included total volume, bone volume, trabecular number, trabecular thickness and trabecular spacing (Table 2.3). These parameters were selected as they represent the 3D model of trabecular bone microarchitecture (Bouxsein, 2010). Both proximal and distal portions were used to evaluate whether there were changes that occurred to the whole bone.

Table 2.3: Definition and description of outcomes from µCT scans

Variable	Description	Standard unit
Total volume	Volume of the entire region of interest	mm^3
Bone volume	Volume of the region segmented as bone	mm^3
Trabecular number	Measure of the average number of trabeculae per unit length	1/mm
Trabecular thickness	Mean thickness of trabeculae	Mm
Trabecular separation	Mean distance between trabeculae	Mm

Measurements were taken using VGSTudio Max 3.0 (Volume Graphics®). A histogram was used to exclude the grey values that represented the container the humeri were packaged in. In the preview, sections representing the air were excluded to reduce the processing power needed in the analysis. Bicondylar breadth was measured by selecting the calliper tool under the instruments tab. Surface determination was applied to confirm that the background that was removed did not compromise the sample material. The region of interest was then selected for surface determination and subsequently, the variables (Table 2.3) were obtained under the morphometrics tab on VG Studio. The measurements obtained helped in establishing whether there were differences in BMD by STA status (Appendix I).

2.3 Data analysis

The data were managed in Microsoft Excel 2007 (Microsoft Corporation) after they were collected using VGStudio Max 3.0 (Volume Graphics®) for the µCT analysis and Olympus CellSens™ and ImageJ® for the histological sections. Data were analysed using SPSS® version 23 (IBM®).

Descriptive statistics for all measurements were generated. The primary investigator's ability to repeat the measurements and the ability of an independent observer to repeat the measurements were assessed using Lin's (1989) concordance correlation of reproducibility on 10 randomly selected samples. Outliers were identified using the outlier labelling rule that is used to identify outliers in samples of univariate data for both symmetric and asymmetric data. The adjusted outlier labelling rule is especially relevant for smaller samples (Hoaglin & Iglewicz, 1987). Histograms and the Shapiro Wilk test were used to test for normality of the quantitative data from the histological sections as well as the µCT scans.

To assess the difference between the mean measurements for the control and STA groups, independent-sample t-tests were conducted, followed by a one-way ANOVA. The difference of means of measurements between the anterior and posterior plates in the control group with a translucent septum was assessed using a one-sample t-test (Park, 2009). Two possibilities arose from the one-sample t-test. The first possibility occurred if the difference of measurements were significantly different from the test value of 0. Then no further tests were conducted as the measurements were statistically different from one another. The second possibility emerged if the difference of measurements were not significantly different from the test value of 0, indicating similarity between measurements. When this occurred Bland-Altman scatter plots were constructed and a linear regression was performed. The Bland-Altman plots were used to indicate the differences of measurements as well as to indicate the presence of systematic bias and identify possible outliers. This method plots the differences of measurements against the average of the two measurements and relies on the repeatability of the measurements (Bland & Altman, 1986). The linear regression was performed in order to expand upon the Bland-Altman plots, such that bias of measurements above and below the mean of the measurements was assessed.

For the density measurements, bone area and connective tissue area in the three groups were compared using a one way ANOVA. To compare the bone area to connective tissue area, t-tests were done for each group. T-tests were also conducted to compare anterior to the

posterior density of connective tissue. Scatterplots of the anterior and posterior bone densities were constructed to visualise the differences and an ANOVA was conducted.

2.4 Ethics

This research is covered by the National Health Act no. 61 of 2003, which allows for the use of human tissues for research and teaching purposes (W-CJ-101109-1) (National Health Act, 2003). Permission to use the Cadaveric Teaching Collection and the RA Dart Collection of Human Skeletons was granted by the Collections Committee of the School of Anatomical Sciences, University of the Witwatersrand (Appendix J).

Chapter 3

Results

3.1 Histomorphometric analysis of the STA

3.1.1 Tissue composition of sections

The tissue in the STA was composed of dense regular connective tissue, containing both collagen fibres and fibrin. This connective tissue was attached tightly to the surrounding bone (Fig. 3.1B). The opaque septum group exhibited bone throughout, in the form of both trabecular and cortical bone (Fig. 3.2). The translucent septum sections had connective tissue on the anterior and posterior aspects with bone throughout the section (Fig. 3.3).

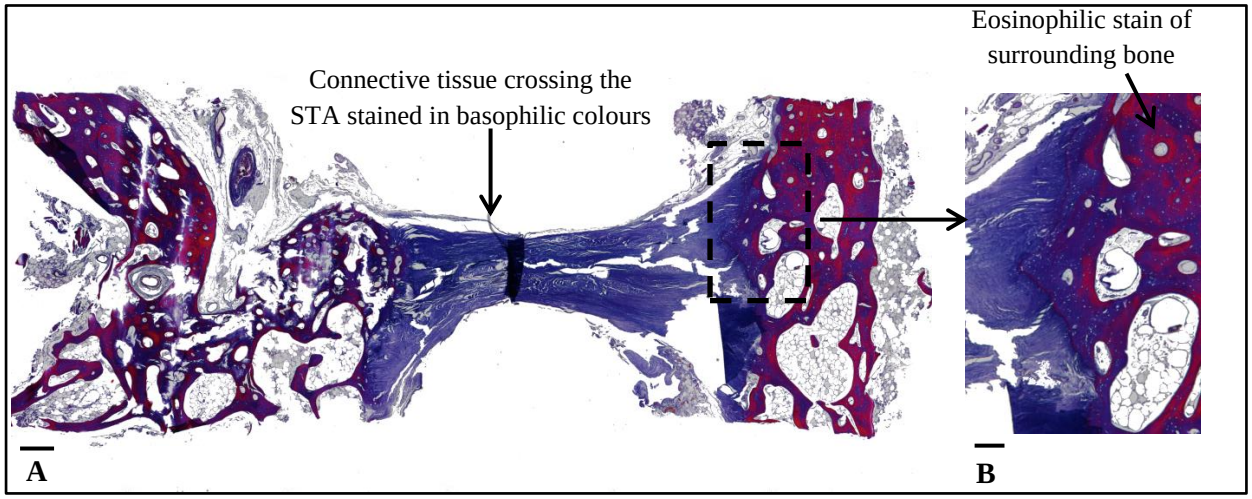


Figure 3.1: STA (composite image) stained with rapid one-step mallory heidenhain

A. Tissue that occupies the STA displays an abundance of connective tissue arranged in a regular manner, as represented basophilic colours. Bone is seen surrounding this connective tissue as depicted in eosinophilic colours. Scale bar = 500 µm. 10x magnification
B. A higher magnification showing the attachment of connective tissue to bone. Scale bar = 150 µm.

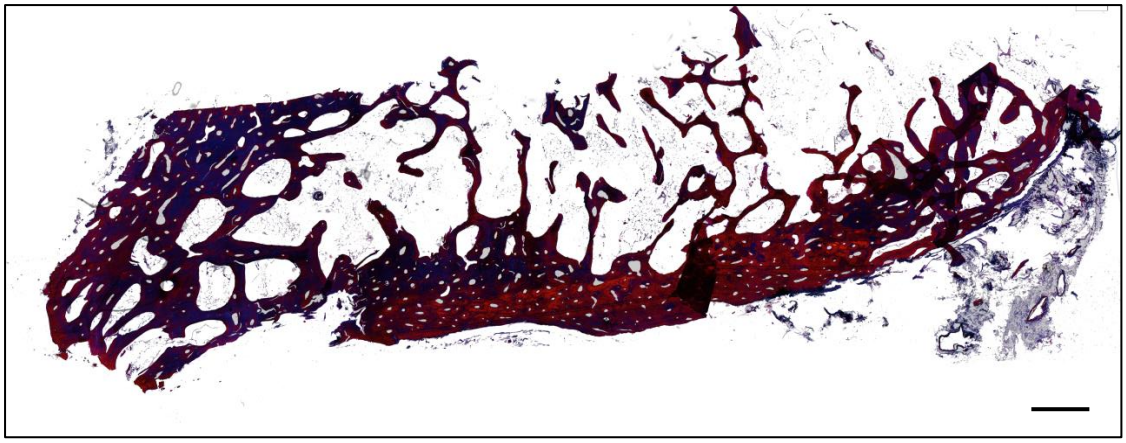


Figure 3.2: Opaque septum sample (composite image) stained with rapid one-step mallory heidenhain. The STA is absent as indicated by the presence of bone throughout the section. Scale bar = 1 mm.

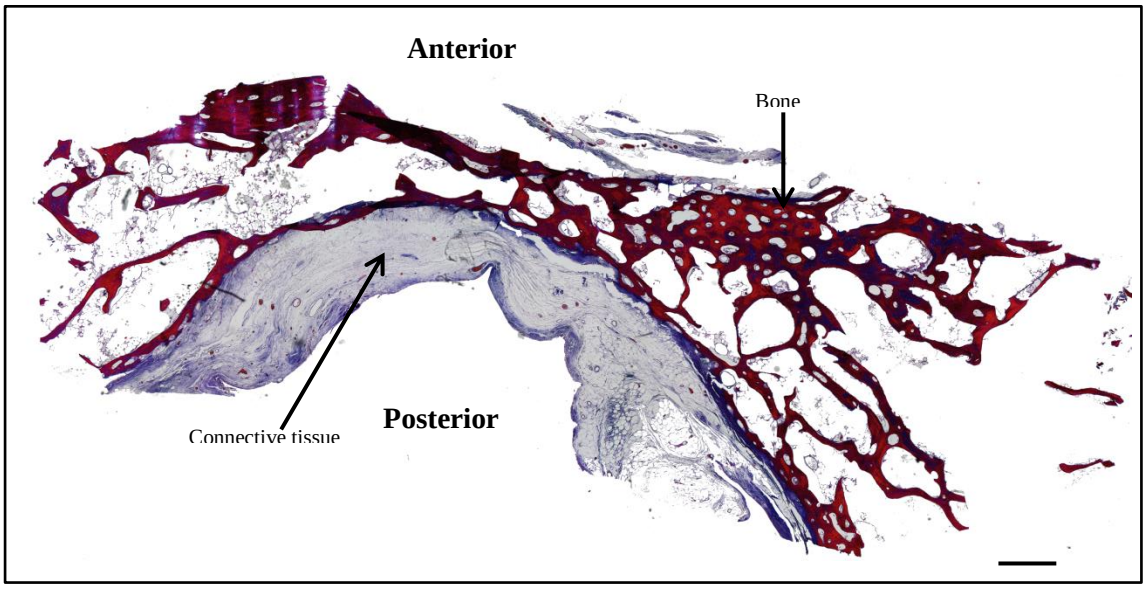


Figure 3.3: Translucent septum sample (composite image) stained with one-step mallory heidenhain. A substantial amount of connective tissue is present on either side of the bone, making the septum appear translucent on X-ray. Scale bar = 1 mm.

Upon further inspection of the picrosirius red staining of the connective tissue present in the STA and translucent septum sections, it was found that the tissue contained both Collagen Type I (represented in dark orange, red and shades of pink) and Collagen Type III (represented in light orange, yellow and in certain slides, green/ blue) as seen in Figure 3.4.

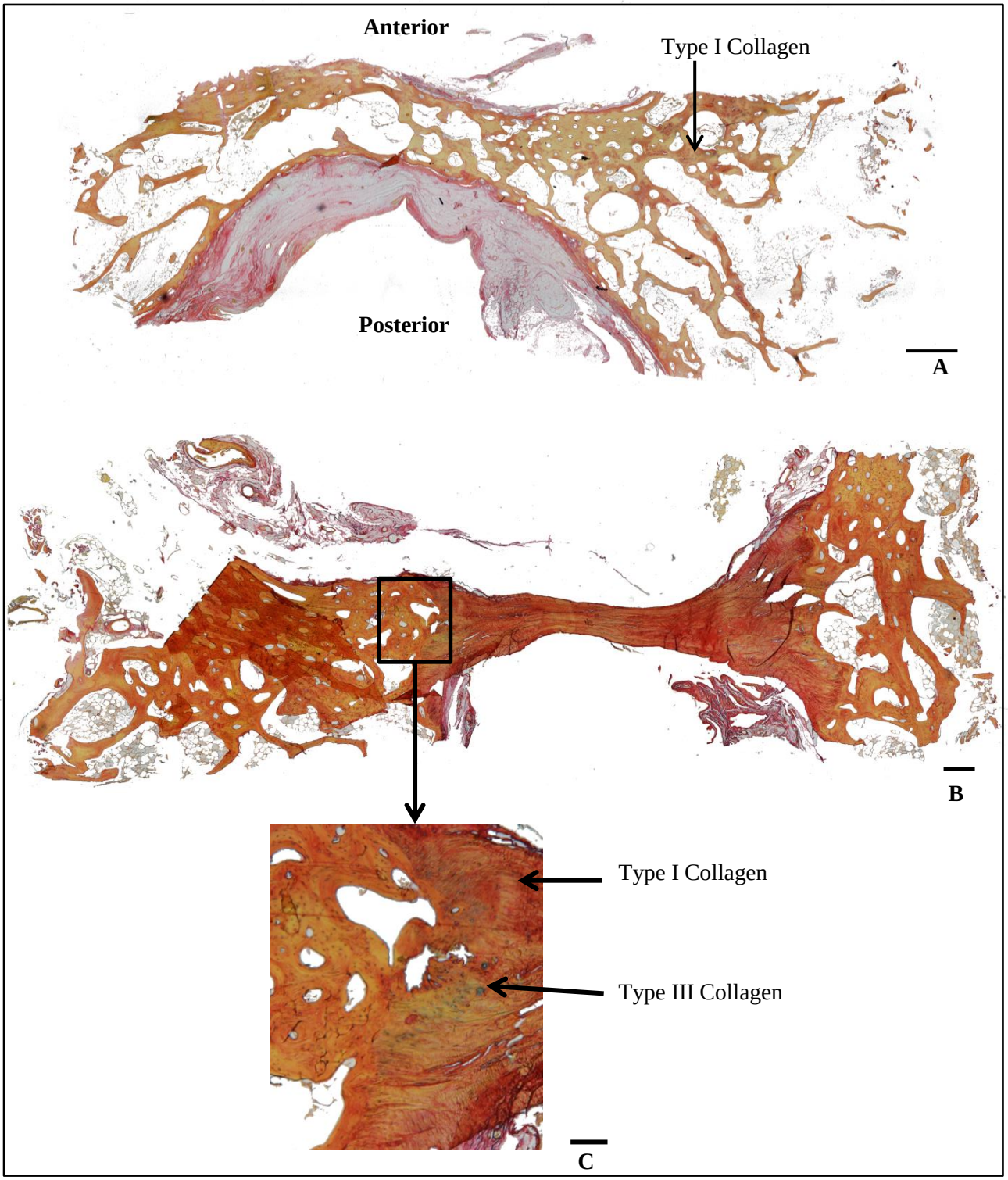


Figure 3.4: Translucent septum and STA present sections (composite image) stained with picrosirius red. A: Translucent septum section stained with Picrosirius red indicating the formation of connective tissue on the anterior and posterior aspects of the section. Scale bar = 1 mm.

B: STA present section stained with picrosirius red indicating the presence of Collagen Type I and Collagen Type III. Scale bar = 1 mm.

C: A higher magnification, indicating the staining of the Collagen Type I and Type III on the section. Scale bar = 0.25 mm.

3.1.2 Quantitative results

Measurement repeatability

Lin's (1989) concordance correlation coefficients (P_c) for all the measurements are provided in Table 3.1. All measurements had a P_c value greater than 0.9 which are considered to be repeatable (Lin & Torbeck, 1998; Goto & Mascie-Taylor, 2007).

Outliers

Outliers were identified using the adjusted outlier labelling with g = 2.2, as this value is adjusted for small sample sizes such as the one in this study. All data fell within the acceptable range (Hoaglin & Iglewicz, 1987)

Normality

The results from the Shapiro Wilk test indicate that all data were normally distributed, as there were few outliers.

Table 3.1: Lin's concordance correlation coefficients of reproducibility (P_c) for intra- and inter-observer repeatability of histomorphometric measurements

Variables	Intra-observer	Inter-observer
Whole Section Area	0.99852	0.99951
Whole section Length	0.99956	0.99987
Width at 25th Percentile	0.99888	0.99771
Width at 50th Percentile	0.99759	0.99668
Width at 75th Percentile	0.99908	0.99975
STA length	0.99936	0.99902
STA Width at 25th Percentile	0.99671	0.99379
STA Width at 50th Percentile	0.99712	0.99582
STA Width at 75th Percentile	0.98536	0.98810
Area of STA	0.98507	0.96712
Anterior plate length	0.95838	0.90927
Anterior plate width at 25th percentile	0.95277	0.95198
Anterior plate width at 50th percentile	0.98307	0.98717
Anterior plate width at 75th percentile	0.96773	0.93079
Anterior plate area	0.98991	0.98542
Posterior plate length	0.97570	0.93928
Posterior plate width at 25th percentile	0.95320	0.96152
Posterior plate width at 50th percentile	0.96126	0.95886
Posterior plate width at 75th percentile	0.95406	0.91566
Posterior plate area	0.99818	0.99639
Bone area from Picrosirius Red stains	0.99359	0.99763
Connective tissue area from Picrosiriuis Red stains	0.99911	0.98710

Descriptive statistics

Table 3.2 provides descriptive statistics for the variables investigated. There is high variation particularly with the whole section area measurement (mean =125.81±81.52), area of STA (mean = 29.94±18.11), bone area (mean = 30.13 ± 11.22) and total connective tissue (mean = 8.63 ± 8.74) due to the differences between the groups measured. There is variation in the connective tissue posterior plate (mean = 5.95±3.54) due to the differences between the translucent septum sections and opaque septum sections.

Table 3.2: Descriptive statistics of histomorphometric measurements (mm)

Variables	N	Min	Max	Mean	SD
Whole section area	31	23.55	433.04	125.81	81.52
Whole section length	31	8.94	19.94	13.83	2.11
Width at 25th percentile	31	1.20	4.92	3.29	0.95
Width at 50th percentile	31	1.15	5.56	3.00	1.20
Width at 75th percentile	31	0.78	5.56	3.63	1.09
STA length	10	4.24	9.95	6.71	1.57
STA width at 25th percentile	10	0.72	4.00	2.16	1.21
STA width at 50th percentile	10	1.00	2.99	1.66	0.66
STA width at 75th percentile	10	1.12	4.52	1.97	1.05
Area of STA	10	10.11	72.47	29.94	18.11
Anterior plate length	7	2.78	6.99	4.85	1.59
Anterior plate width at 25th percentile	7	0.02	1.36	0.54	0.42
Anterior plate width at 50th percentile	7	0.17	1.31	0.50	0.39
Anterior plate width at 75th percentile	7	0.13	1.05	0.60	0.29
Anterior plate area	7	1.20	5.61	2.30	1.63
Posterior plate length	10	5.85	9.87	7.25	1.24
Posterior plate width at 25th percentile	10	0.15	2.09	1.04	0.72
Posterior plate width at 50th percentile	10	0.20	2.11	0.98	0.69
Posterior plate width at 75th percentile	10	0.24	2.65	1.05	0.74
Posterior plate area	10	2.88	14.40	6.50	3.57
Bone area	31	0.02	46.86	30.13	11.22
Total connective tissue	26	2.46	17.86	8.63	8.74
Connective tissue posterior plate	21	1.83	14.29	5.95	3.54
Connective tissue anterior plate	18	0.35	7.63	2.56	1.90

Measurement of bone volume

The volume of bone in the groups showed significant differences between the opaque septum and STA present groups (p = 0.031). Similarly, a significant difference was found between the opaque and translucent septum groups (p = 0.038). The bone volume between the translucent septum and STA present group showed a significant difference (p = 0.041) as seen in Table 3.3. The bone volume of the opaque septum group was variable in terms of the area of bone. The smallest area was 7.49 mm^2 and the largest area was 46.86 mm^2. The opaque septum group ranged from septa that had a large amount of the cortical bone and very little trabecular bone (Fig. 3.5A) to septa containing sparse amounts of cortical bone and greater amounts of trabecular bone occurring between cortical bone (Fig 3.5B).

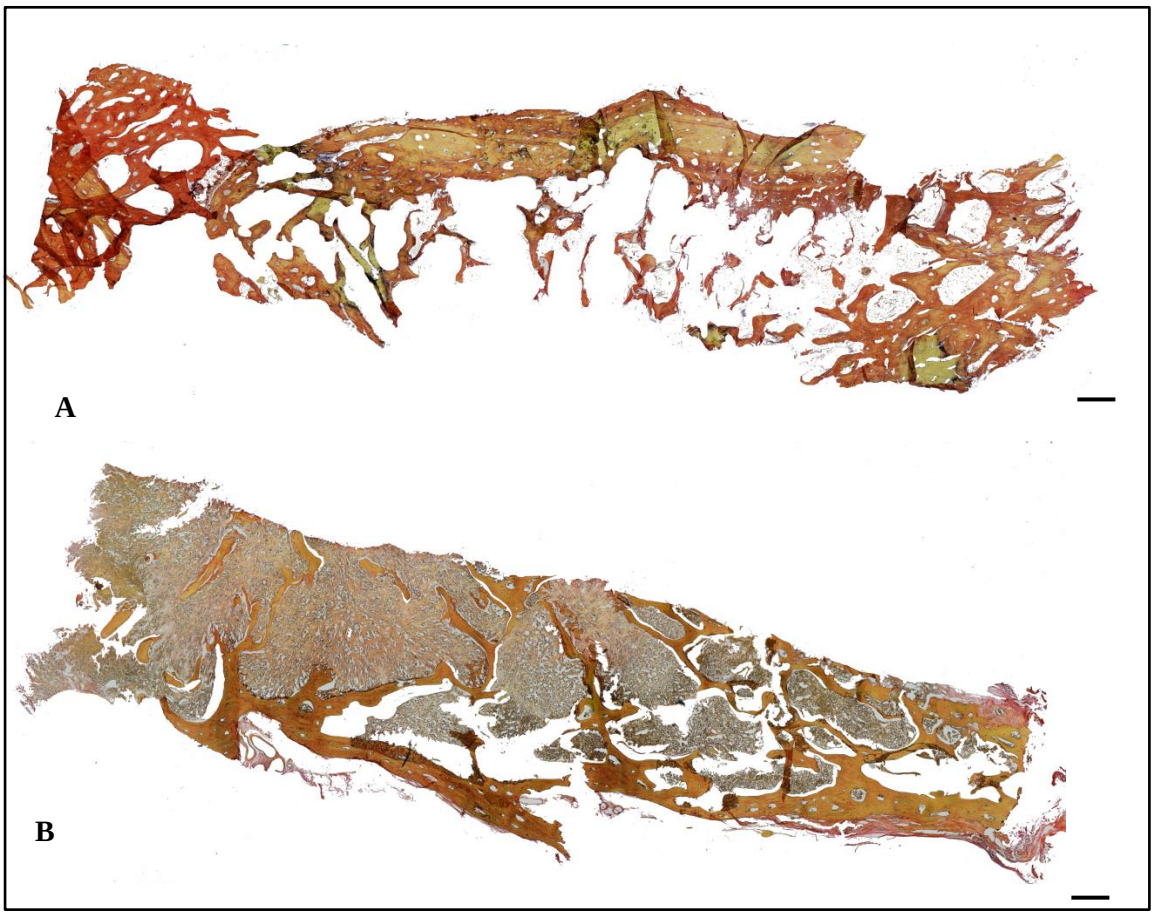


Figure 3.5: Opaque septum sample (composite image) stained with picrosirius red

A. Opaque septum with a greater volume of cortical bone. Scale = 500 µm. 10x magnification
B. Opaque septum with a greater volume of trabecular bone. Scale = 500 µm. 10x magnification

Table 3.3: Results of the independent samples t-tests for measurements of bone area

Variables	N	Mean diff.	SD*	P-value	r-value
Difference of means opaque vs STA present bone area	21	4.67106	4.55403	0.031	-
Difference of means opaque vs translucent septum bone area	21	-1.68836	9.92995	0.038	0.825
Difference of means STA present vs translucent septum bone area	20	2.98270	3.95797	0.041	-
Difference of means bone vs CT area	26	4.16265	8.07443	0.014	-

Measurement of bone volume – Anterior vs. Posterior

Figure 3.6 Indicates the distribution of bone in translucent septum measurements, group 1 representing the most posterior 20th percentile and group 5 representing the most anterior 20th percentile.

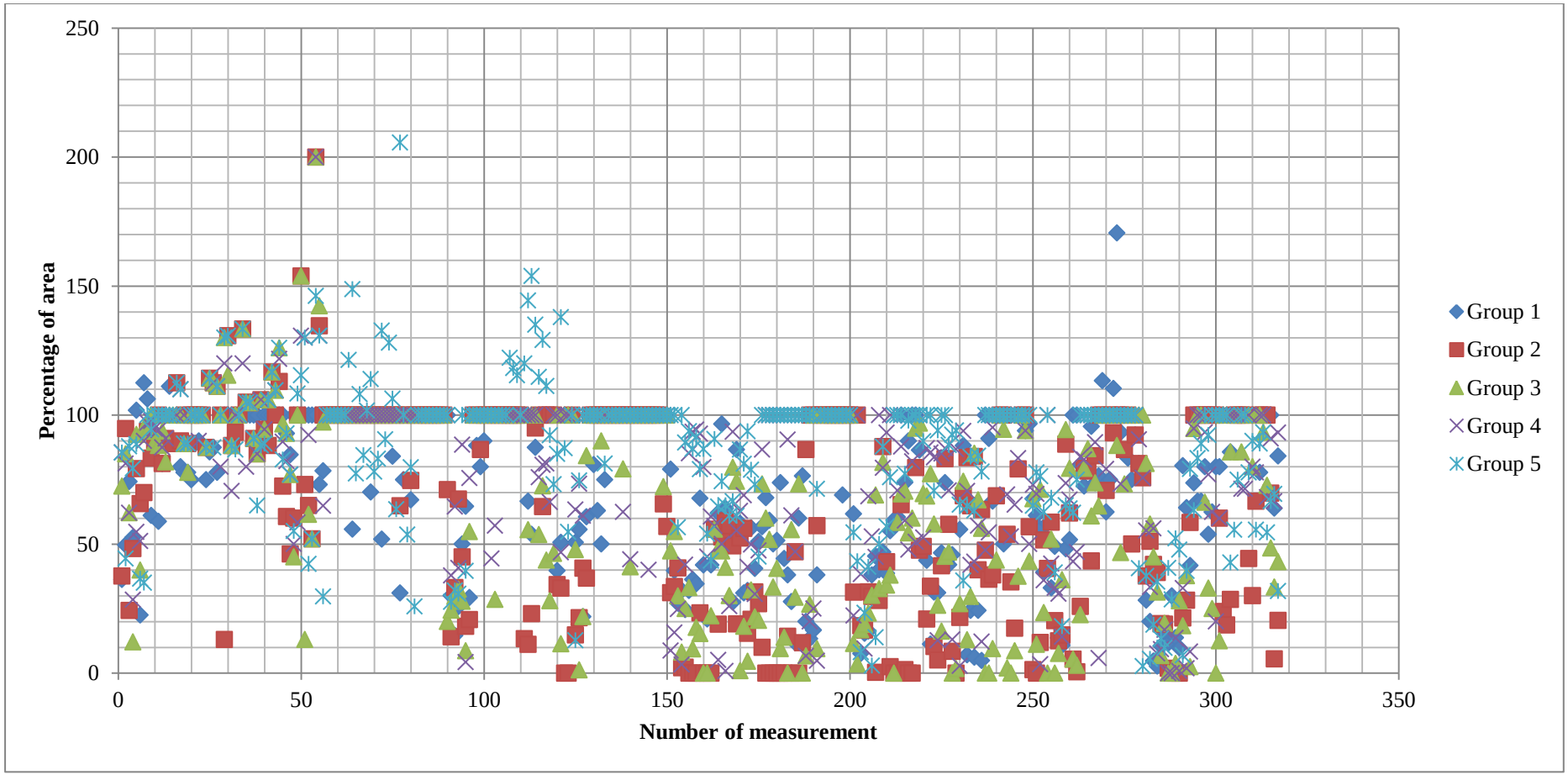


Figure 3.6: Distribution of bone in translucent septum sections when divided into percentiles.

Figure 3.7 indicates the mean percentage of bone area. Group 2 which represents the 40th percentile has the lowest mean percentage of area (66.88mm^2) while group 5 representing the 81st to 100th percentile, and is the most anterior aspect of the section, has the highest mean percentage of area (87.26mm^2).

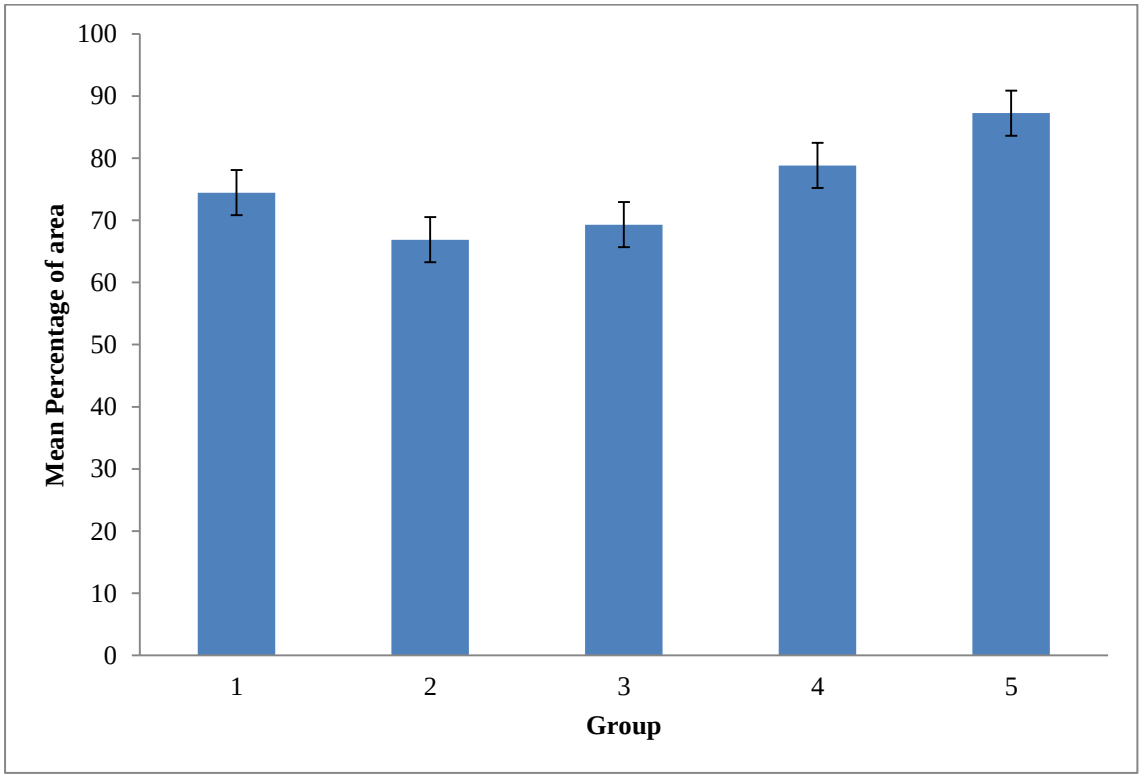


Figure 3.7: Mean percentage of area occupied by bone on translucent septum sections, divided into 20th percentiles from posterior to anterior. Group 1 represents the 1st 20th percentile (the most posterior) and group 5 represents the 5th 20th percentile (the most anterior of the section).

Figure 3.8: The distribution of bone in opaque septum measurements.

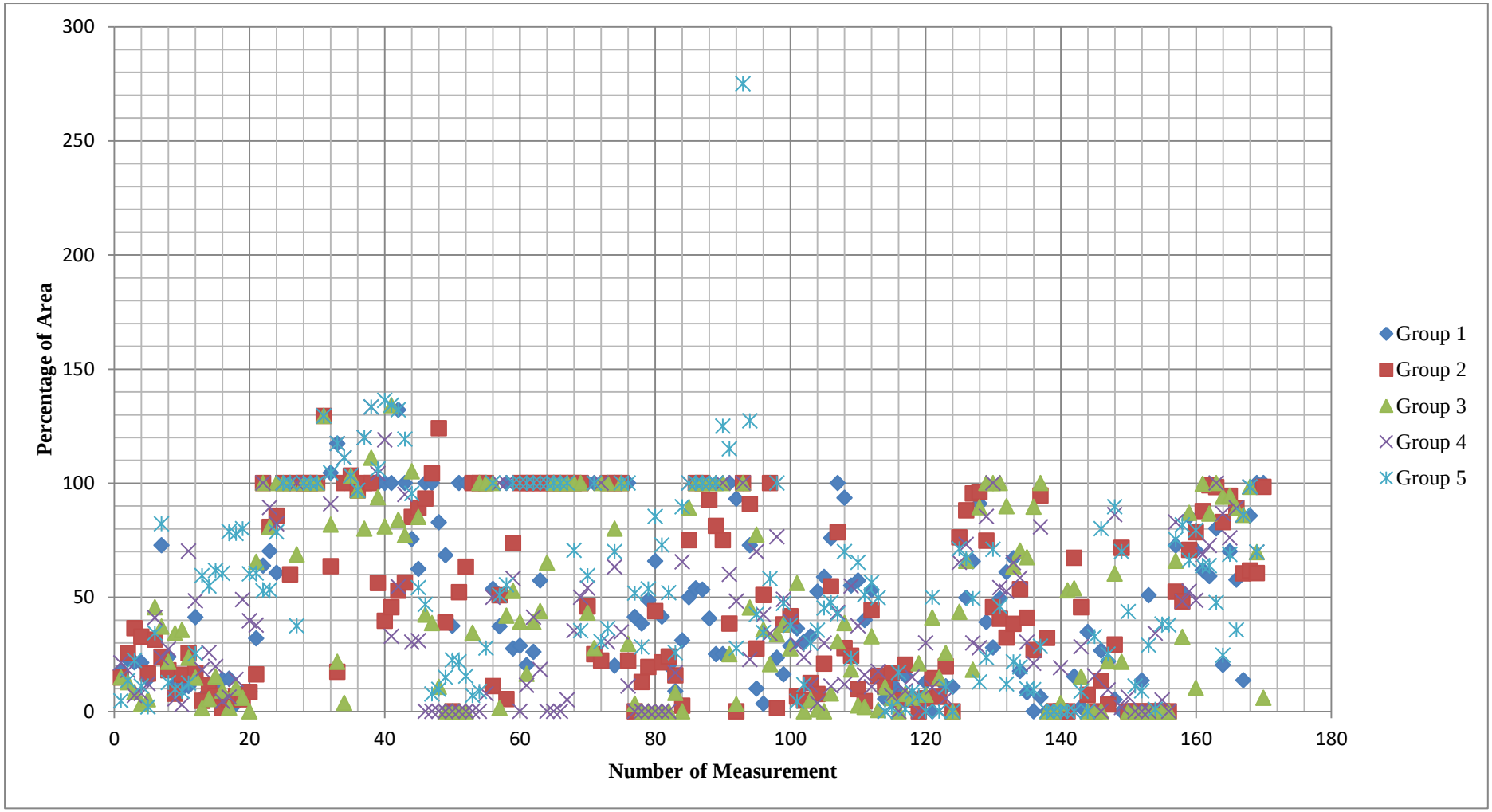


Figure 3.8: Distribution of bone in opaque septum sections when divided into percentiles.

Figure 3.9 indicates the mean percentage of bone area. Group 4, which represents the 80th percentile, has the lowest mean percentage of area (42.27 mm^2) while group 5 (the 81st to 100th percentile, and the most anterior aspect of the section), has the highest mean percentage of area (56.18 mm^2).

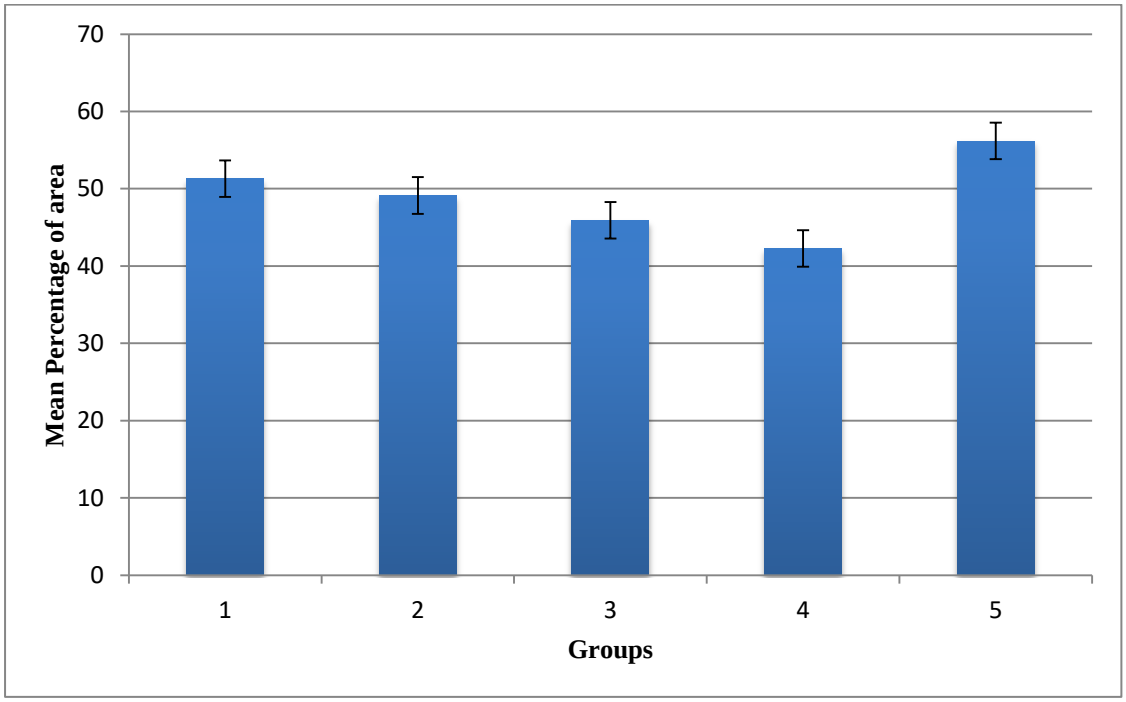


Figure 3.9: Mean percentage of area occupied by bone on opaque septum sections, divided into 20th percentiles. Group 1 representing the 1st 20th percentile being the most posterior and group 5 representing the 5th 20th percentile being the most anterior of the section.

Figure 3.10 shows that there is a marked difference between the anterior and posterior bone area between the translucent and opaque septum groups when comparing plate resorption ($p = 0.003$).

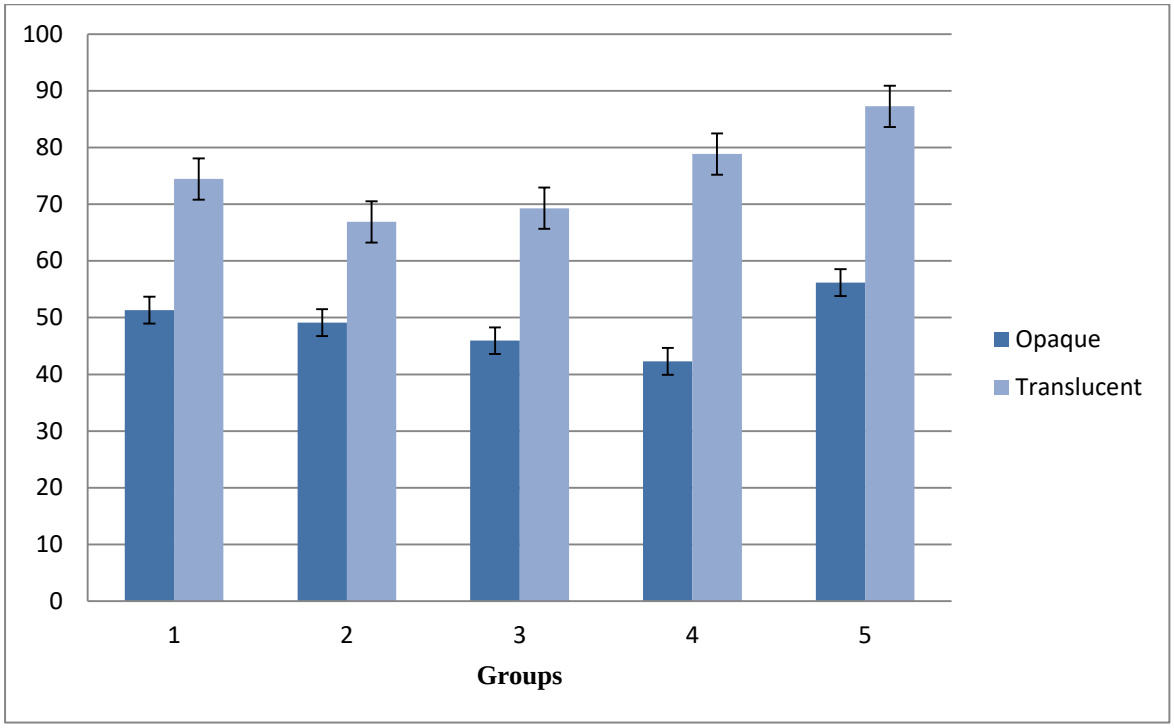


Figure 3.10: Difference between opaque and translucent septum sections in the measurement of bone area, comparing anterior to posterior density.

Measurement of connective tissue area

There was a significant difference in connective tissue area between the opaque septum and STA present groups ($p=0.004$) and between the opaque and translucent septum groups ($p=0.015$). Furthermore, there was no significant difference between the STA present and translucent septum groups ($p = 0.864$) (Table 3.4).

Table 3.4: Results of independent samples t-tests for connective tissue area

Variables	N	Mean diff.	SD*	P-value	r-value
Difference of means Opaque vs STA present CT area	17	-0.50925	2.25917	0.004	-
Difference of means Opaque vs Translucent septum CT area	17	0.32792	2.44913	0.015	-
Difference of means STA present vs Translucent septum CT area	18	-0.18133	2.40836	0.864	0.525
Difference of means Bone vs CT area	26	4.16265	8.07443	0.014	-

The translucent septum sections had connective tissue on the anterior and posterior aspects of the septum with bone in between (Fig. 3.11).

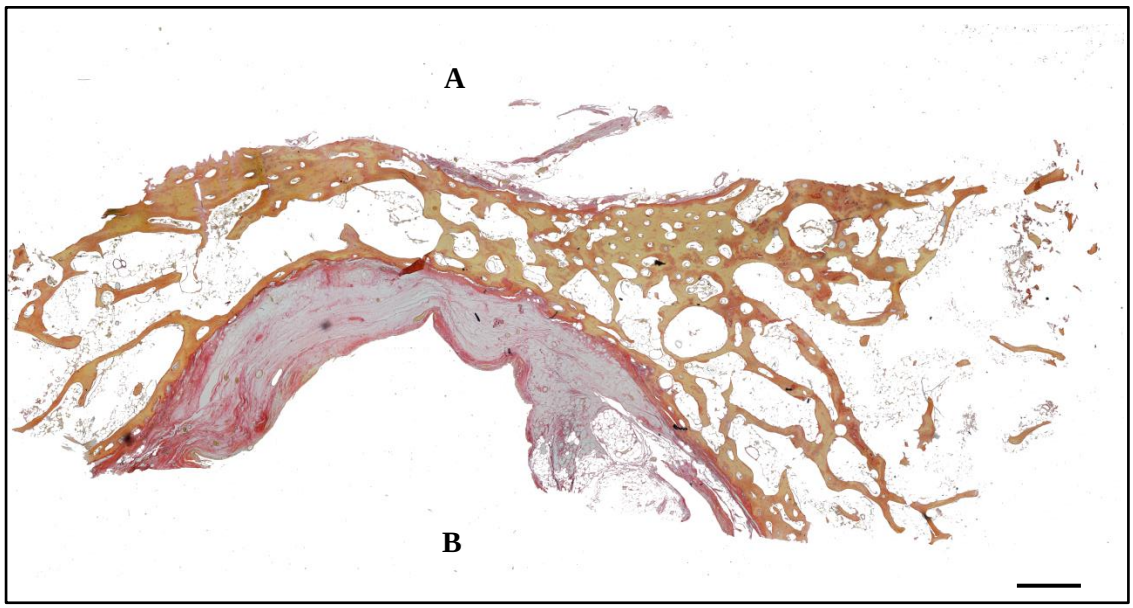


Figure 3.11: Translucent septum sample (composite image) stained with picrosirius red indicating connective tissue formation on the (A) anterior and (B) posterior aspects. Scale = 1mm.

Table 3.4 indicates that there was a significant difference (p = 0.014) between the average area of the connective tissue (8.63mm) and the average area of bone (14.92mm).

Anterior vs. posterior connective tissue area

There was a significant difference between the area of connective tissue found on the posterior aspect of the septum compared to the anterior aspect in translucent septum sections (p = 0.003) as illustrated by Fig. 3.12, indicating that the average area of connective tissue on the posterior aspect (5.95mm) was greater than the average area of connective tissue on the anterior aspect (2.20mm).

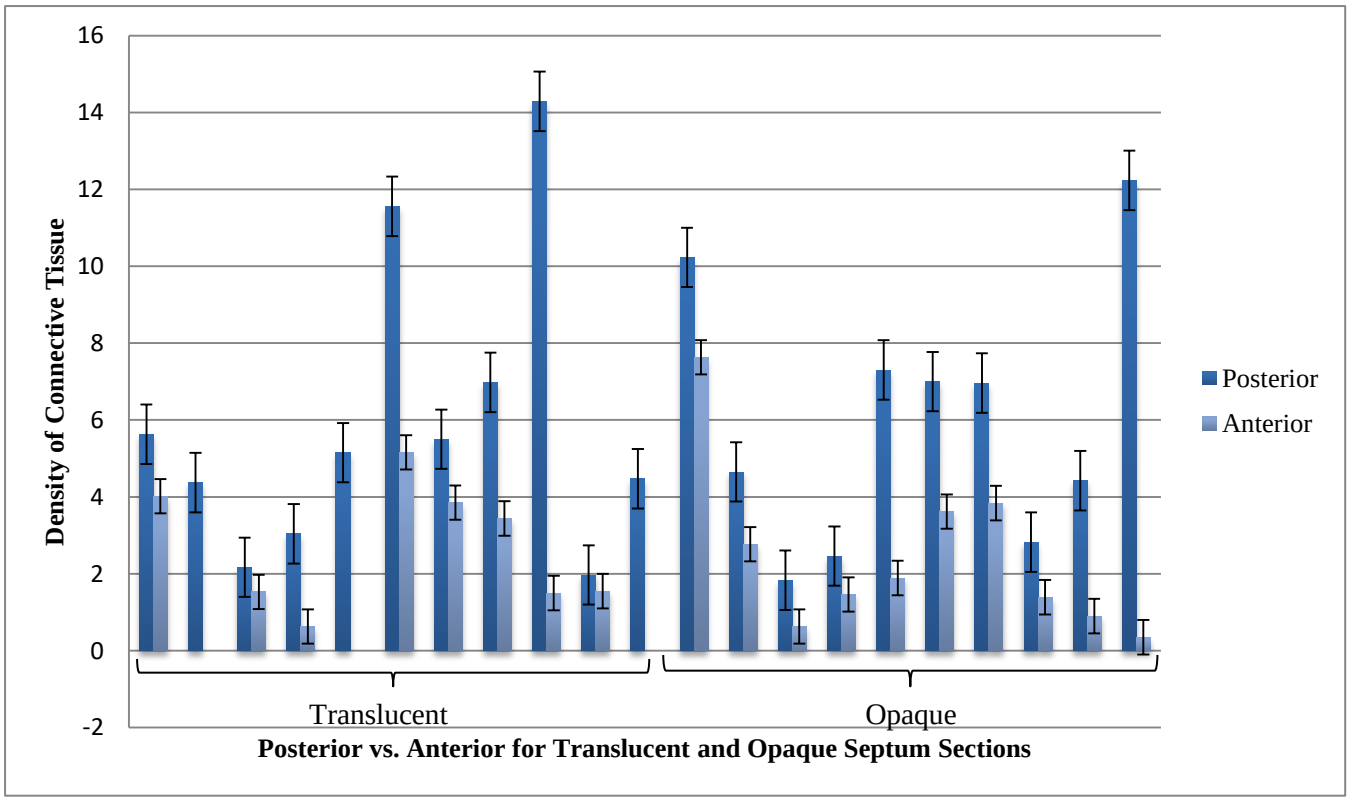


Figure 3.12: Differences between the connective tissue area on the anterior and posterior aspects of translucent and opaque septum sections.

3.2 Morphological properties of humeri with and without the STA

3.2.1 Bicondylar breadth

When the STA was absent on the left arm we observed a marginally lower bicondylar breadth than when the STA was present (Fig. 3.13). However, these differences were not significant (p=0.69). Conversely, on the right side, the bicondylar breadth was marginally lower when the STA was present than when the STA was absent. Again no significant level of difference was detected (p=0.90) (Figure 3.13).

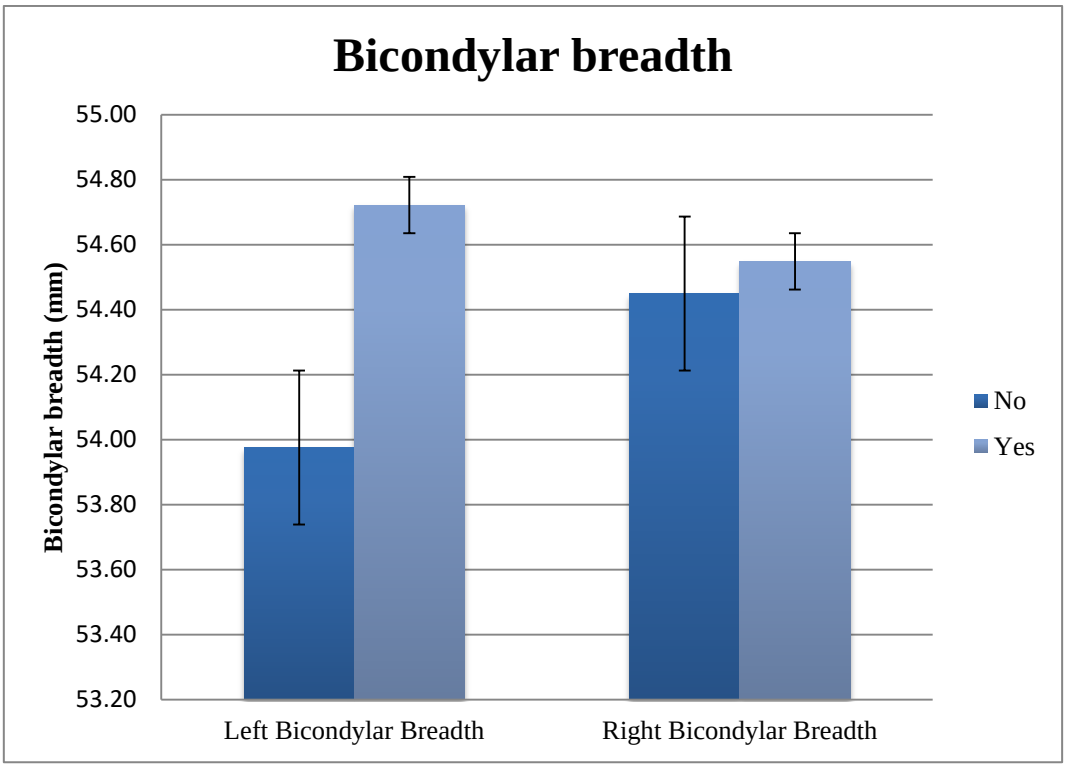


Figure 3.13: Left and right bicondylar breadth measurements. No: STA absent. Yes: STA present.

3.2.2 Bone to total bone volume ratio (BV/TV)

The bone to total bone volume ratios (BV/TV) were evaluated by location and side, whereby BV/TV was measured in the proximal and distal regions of both the left and right humeri of individuals. In the proximal region on the left side, the ratio was lower when the STA was present as seen in Figure 3.14. In contrast, the values were almost identical for the distal

region. On the right side, the BV/TV values were similar for both STA statuses and both regions (Figure 3.14).

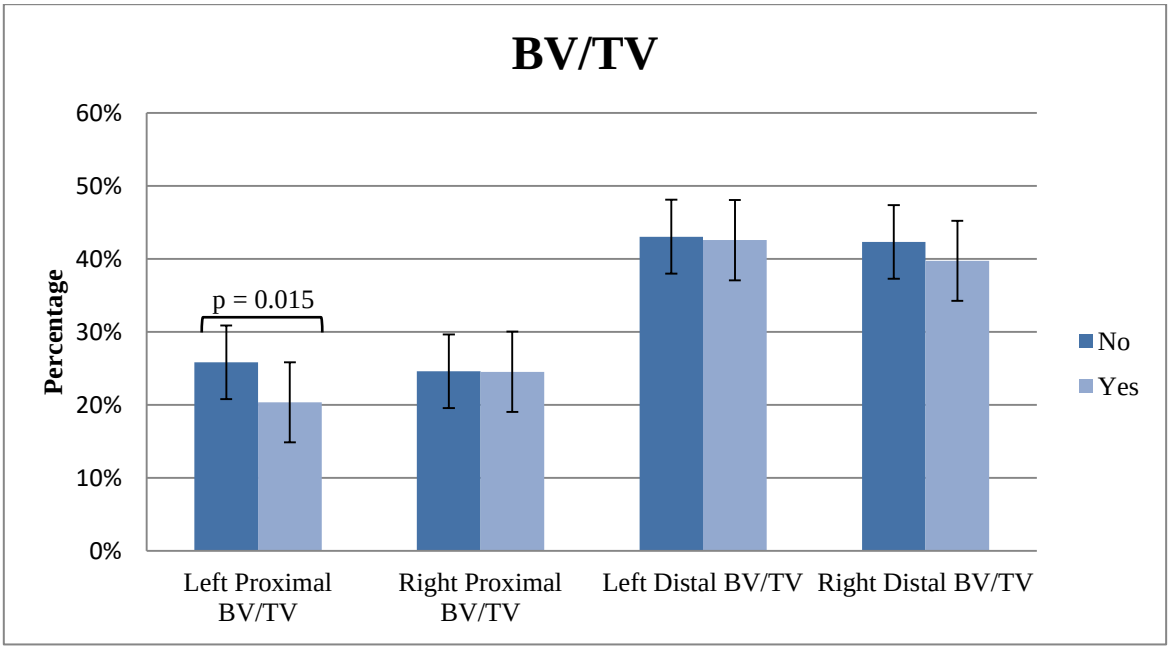


Figure 3.14: Ratio of bone volume to total volume (BV/TV) of proximal and distal humeri according to STA status. No: STA absent. Yes: STA present.

3.2.3 Trabecular thickness (TbTh)

No group differences in trabecular thickness (TbTh) were observed in the proximal and distal extremities of the left humerus. In the proximal region, trabecular thickness (TbTh) was marginally lower when the STA was present (p=0.44 between the two groups). In the distal region, the trabecular thickness was also similar in the two groups

On the right side, the proximal trabecular thickness (TbTh) was similar when the STA was present or absent (p=0.87). Although, in the distal region, the trabecular thickness was marginally lower when the STA was present (Figure 3.15).

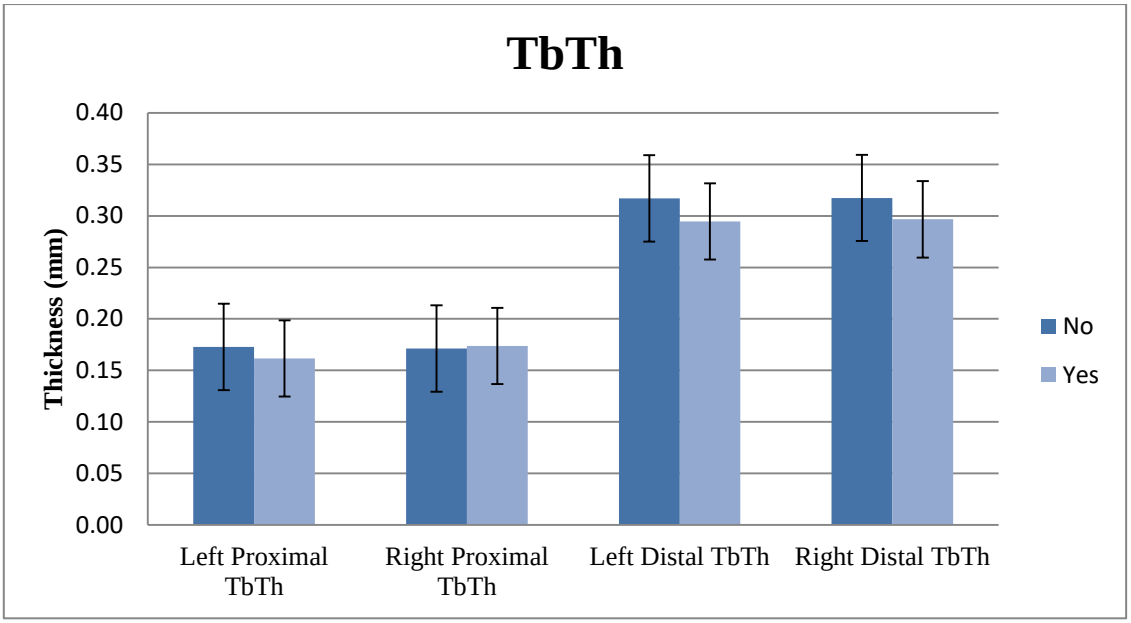


Figure 3.15: Trabecular thickness (TbTh) of proximal and distal humeri according to STA status. No: STA absent. Yes: STA present.

3.2.4 Trabecular number (TbN)

On the left side, with respect to trabeculae number (TbN), the proximal region exhibited fewer trabeculae when the STA was present ($p=0.004$ between the two groups) as indicated in Figure 3.16. In the distal region, the trabecular number (TbN) when the STA was present was marginally higher, however, no significant difference between the two groups was detected ($p=0.55$).

On the right side, in the proximal region, the trabecular number (TbN) was not statistically different when the STA was present or absent ($p=0.72$). Similarly, in the distal region, the trabecular number (TbN) when the STA was present was marginally higher than when the STA was absent, however, no significance was detected ($p=0.78$) (Figure 3.16).

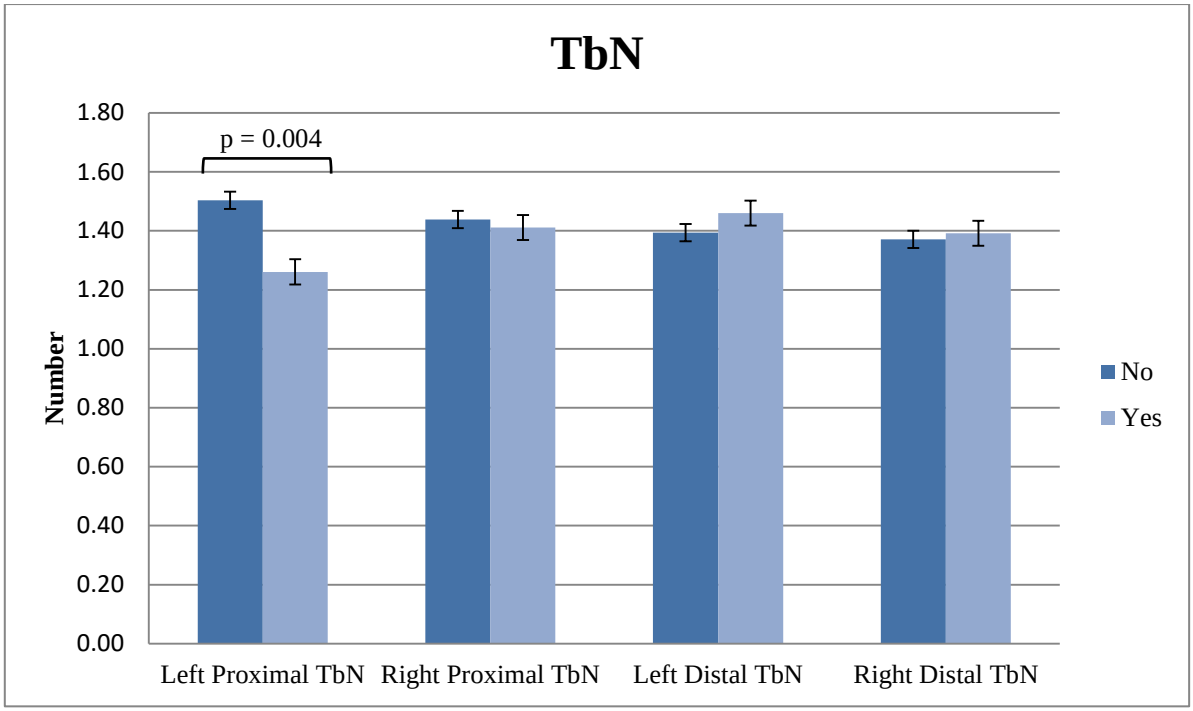


Figure 3.16: Trabecular number (TbN) of proximal and distal humeri according to STA status. No: STA absent. Yes: STA present.

3.2.5 Trabecular spacing (TbSp)

On the left side, in the proximal region, trabecular spacing was wider when the STA was present compared to when the STA was absent (p=0.05 between the two groups) as seen in Figure 3.17. Conversely, in the distal region, no significant difference was found between the two groups (p=0.67).

On the right side, in the proximal region, no significant difference was found for the trabecular spacing between the two groups (p=0.83). This pattern continued in the distal region, where no significant difference was found between the two groups (p=0.41) (Figure 3.17).

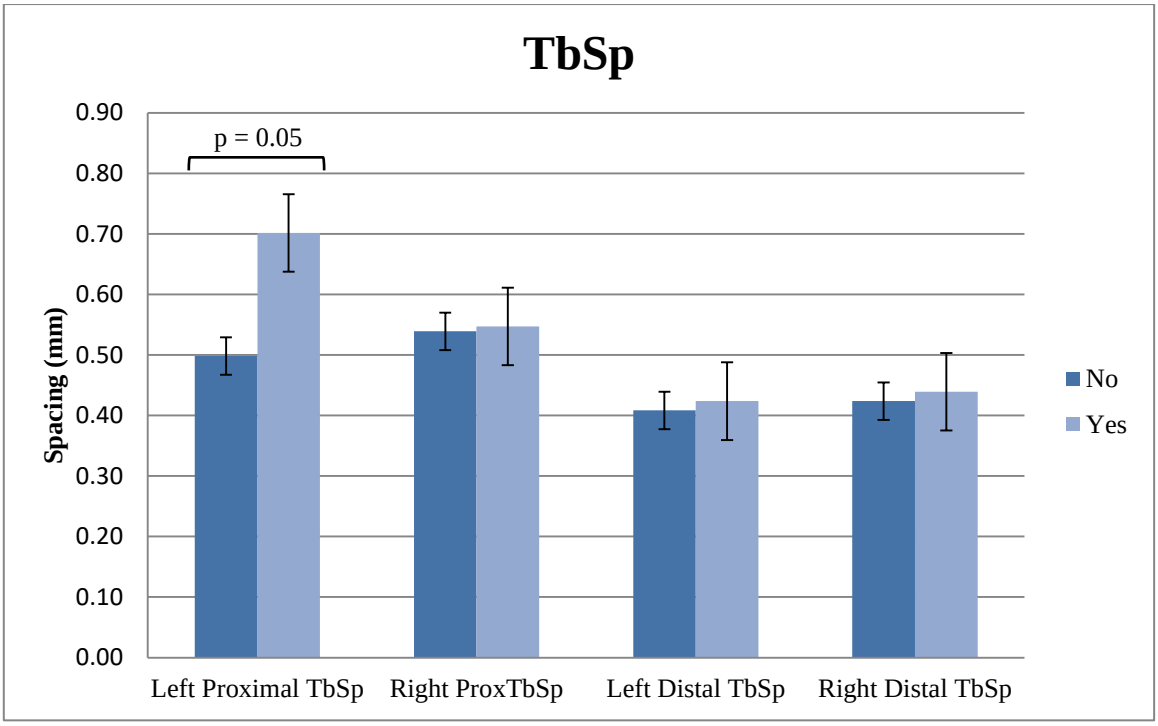


Figure 3.17: Trabecular spacing (TbSp) in the proximal and distal humerus according to STA status. No: STA absent. Yes: STA present.

Chapter 4

Discussion

This study employed histological techniques and Micro-Focus X-Ray Computed Tomography (µ-CT) to document and compare differences in the internal bone morphology and tissue composition in the septum between the coronoid and olecranon fossae. The histological aspect of the study focused on the distal portion of the humerus, particularly the bony septum that separates the olecranon and coronoid fossae or the STA region. The trabecular morphology of humeral proximal and distal epiphysis was explored through µ-CT. The combination of the two levels of analysis enabled us to address, in a novel way, key questions regarding the formation and composition of the STA region tissues and the osseous characteristics of humeri with and without the STA.

We proposed that the bony septal plate would be resorbed primarily from the posterior aspect in STA formation due to impingement by the ulnar olecranon process. The plausibility of this theory was tested by measuring and comparing the density of the connective tissue present on the anterior and posterior aspects of sections with the STA, bone sections with a translucent septum and those with an opaque septum. To understand the relationship between poor trabecular morphological properties in bones with the STA, µCT was utilized to quantify trabecular thickness, number, size and estimation of the volume of the trabecular bone.

4.1 Tissues crossing the STA

As is well documented, there are no anatomically functional structures that pass through the STA and none were found in this study. Ndou *et al.* (2018) found that dense regular connective tissue encompasses the gap created by the bone deficient septum in STA cases. Dense regular connective tissue is generally found in tendons and ligaments for structural support and strength. The dense regular connective tissue may function to provide strength and support as the septum is usually composed of bone. As in previous findings (Ndou, 2015), collagen and fibrin are both observed in the connective tissue occupying the STA. Therefore, the type of collagen occupying the STA was of particular interest as the presence of unincorporated collagen type I may indicate incomplete remodelling in response to the pressure from the olecranon process. The result would be bone resorption and osteoblastic secretion of collagen, however, incorporation of hydroxyapatite would not occur, resulting in

the aperture region being able to withstand the continuing pressure from the olecranon in the joint.

The way in which the connective tissue was found to attach to the surrounding bone (Fig. 3.1B) resembles that of a tendon-bone attachment, suggesting the connective tissue provides structural integrity despite the bone deficiency (Ndou *et al.,* 2018). Through the Picrosirius Red stains, it was detected that both Collagen Type I and Type III were present in sections with the STA present and translucent septum sections. The presence of both types of collagen suggests that incomplete bone remodelling occurred in these sections, whereby collagen type I was secreted during the formation stage of bone remodelling, however, it is possible that calcium hydroxyapatite may not have been incorporated to mineralize the bone. Further investigation into calcium hydroxyapatite incorporation would be needed to verify this theory. Collagen type III has been associated with fracture repair and regeneration in various tissues, including bone, due to the increase in its expression following tissue injury (Miedel *et al.,* 2015). However, the specific role that collagen type III plays in tissue healing requires further investigation.

Bone volume

Due to septal resorption caused by micro-cracking of the septum, there is a deficiency of bone in septa that present with the STA (Mays, 2008). In agreement with this, we found a significant difference in the bone area of opaque septum and STA present sections despite the range in the presentation of the opaque septum sections. Furthermore, there was a significant difference between the translucent septum and the STA present sections. This is due to the high bone area present in the translucent septum sections.

It was predicted that the posterior aspect of the bony septal plate would be primarily resorbed due to the actions of the olecranon process, similar to the findings of Ndou & Schepartz (2016). This occurrence was observed through a significant difference in bone area between the anterior and posterior plate, in which a larger bone area was found on the anterior aspect of the bony septum. This is contradictory to the septal resorption theory postulated by Mays (2008), in which septal resorption occurs primarily through the actions of the coronoid process and therefore resorption would occur primarily from the anterior aspect.

Connective tissue area

We found a significant difference in the connective tissue found in STA present sections and translucent septum sections compared to the opaque septum sections. The presence of dense

regular connective tissue found crossing the aperture is a unique feature found in the elbow joint. Since connective tissue serves as mechanical support (Eleswarapu *et al.,* 2011), and dense collagenous connective tissue is found where tensile strength is of paramount importance, the presence of dense regular connective tissue in the STA present and translucent septum sections highlights the need for mechanical strength in that area.

Anterior vs. posterior connective tissue area

Mays (2008) postulated that septal resorption occurs primarily from the anterior aspect of the septum, although the muscles in the anterior compartment of the arm would arguably impede this (Ndou, 2015). In support of Ndou's (2015) argument, we documented a significant difference in the density of connective tissue on the posterior aspect compared to the anterior aspect of the sections, suggesting that resorption occurs primarily from the posterior aspect of the septum.

4.2 Internal osseous morphology of humeri

Bicondylar breadth

There were marginal differences in the bicondylar breadth however no significant differences were found. Ndou & Schepartz (2016) indicated that while bicondylar breadth showed differences when the STA was present to when it was absent, these differences were only significant in the Black and White male South African populations. The lack of significant differences in this study may, therefore, be due to the sample being female.

Trabecular bone

In the present study, we found the bone volume to total volume (BV/TV), trabecular number (Tb.N) and trabecular spacing (Tb.Sp) in the proximal region to be lower when the STA was present on the left side than when the STA was absent. This is in agreement with the findings of Ndou & Schepartz (2016) that there are morphological differences in characteristics of humeri containing the STA. Moreover, Kirschoff and colleagues (2012) indicated that there is an inverse relationship between BV/TV and an individual's age, this was more pronounced in the female population. As this study investigated the microarchitecture of bones with and without the STA in a female population, the role of oestrogen in regulating bone remodelling may have influenced the BV/TV and consequently Tb.N and Tb.Sp. Remodelling is a continuous process and these differences in volume, number and spacing may have come about through the overactivity of bone-resorbing osteoclasts. Increased number and activity

of osteoclasts per bone surface has been linked to bone diseases such as rheumatoid arthritis, osteoarthritis and osteoporosis (Hirayama *et al.,* 2002; Bi *et al.,* 2017). While a correlation between porosity and the STA has been previously found, the relationship between STA formation and osteoarthritic changes is inconclusive, as porosity – indicated by increased Tb.Sp – may be due to several factors (Myszka & Trzcinski, 2015).

No group differences were observed in trabecular thickness (Tb.Th) when the STA was present or absent. However Tb.Th was marginally lower when the STA was present in the distal region on the right side. Tb.Th has been shown to be genetically determined (Paternoster *et al.,* 2013) and therefore oestrogen presence, amongst other factors, may influence the trabecular thickness. Banse and colleagues (2002) correlated the cross-linked profile of bone collagen and the structural organization of trabecular bone and indicated that a high presence of mature collagen cross-links was associated with thin trabeculae that were more numerous and spread over a wide network. This may explain the marginal increase of Tb.N in the distal region when the STA was present.

The predisposition of females to the STA due to their relatively smaller and more gracile bones may also explain the differences found in this study. Glanville (1967) postulated that gracility may genetically predispose individuals to STA formation and development however further research investigation into whether these mechanisms play a role in STA formation and the effects that this may have is needed. McClanahan *et al.* (2002) found that bone area is substantially higher in the dominant arm due to increased mechanical loading regardless of sex, which may explain the side differences observed in this sample; due to the majority of the population being right-arm dominant, the dimensions of these bones would differ and changes would predominantly occur on the smaller bones.

It was considered that discrepancies in the findings may result from factors such as age and also environmental factors affecting bone growth such as nutrition, physical development and genetic factors. Furthermore, the differences in these findings could depend on the differences in the references points taken for these measurements.

Chapter 5

Conclusions

Dense regular connective tissue is found across the space of the STA, the tight arrangement to the surrounding bone suggests that there was a deficit in the structural integrity of the bone and the compensatory method taken to maintain the structural integrity. This deficit may have arisen from incomplete bone remodelling, which can be assumed due to the presence of both Collagen Type I and Collagen Type III.

Through histological analysis, it was shown that septal resorption occurs primarily from the posterior aspect due to the increased occurrence of connective tissue found on the posterior aspect of translucent septum sections compared to that on the anterior aspect. Similarly, there was an increased percentage of bone found on the anterior aspect compared to the posterior aspect of the section in translucent septum sections.

The differences in the BV/TV, TbN and TbSp may be resultant from factors such as overactivity of osteoclasts – pertaining to the theory of incomplete bone remodelling – as well as genetic predispositions. Knowledge of the presence of the STA may aid in surgical procedures (Singhal & Rao, 2007; Paraskevas *et al.*, 2010; Krishnamurthy *et al.*, 2011), in which the medullary canal is shorter and narrower as well as the differences in morphology in the trabeculae in STA present humeri.

5.1 Limitations

The limitations of this study include funding, whereby refinement into more specific collagen types could not be conducted and the sample size for µCT analysis could not be enlarged to the expenses these techniques incurred. Furthermore, a female population was utilised for the analysis of microarchitecture of the humerus, therefore the role of oestrogen may have influenced BMD parameters.

5.2 Recommendations

As this study postulated that the occurrence of the STA may be due to incomplete bone remodelling, long term studies should be conducted to clarify the role of bone remodelling in the aetiology of the STA. Furthermore, studies into the role of different collagen types as well as the structure of collagen in bone remodelling and tissue healing in humeri with and without the STA should be investigated, at different age cohorts. Further studies into the

microarchitecture of the humerus should be conducted on both males and females. Moreover, the overall bone strength of humeri with and without the STA should be investigated. Lastly, research into the relationship between osteoarthritic changes such as porosity, eburnation, etc. and the STA should be investigated as the research thus far has been inconclusive.

References

Akabori, E. (1934). Septal apertures in the humerus in Japanese, Ainu and Koreans. *American Journal of Physical Anthropology*, **18**(8): 395 – 400.

Ammann, P. & Rizzoli, R. (2003). Bone strength and its determinants. *Osteoporosis International* **14**(3): S13 – S18.

Alers, J.C., Kritenburg, P.J., Vissers, K.J. & van Dekken, H. (1999). Effect of bone decalcification procedures on DNA *in situ* hybridization and comparative genomic hybridization: EDTA is highly preferable to a routinely used acid decalcifier. *The Journal of Histochemistry & Cytochemistry* **47**(5): 703 – 709.

Augat, P. & Schorlemmer, S. (2006). The role of cortical bone and its microstructure in bone strength. *Age and Ageing* **35** (Suppl 2): ii27-ii31.

Bakbak, S., Kayacan, R. & Akkuş, O. (2011). Effect of collagen fibre orientation on mechanical properties of cortical bone. *Journal of Biomechanics* **44** (Suppl 1): 11.

Bancroft, J.D. & Gamble, M. (2008)*Theory and Practice of histological techniques.* (5th ed.). London: Churchill Livingstone.

Banse, X., Devogelaer, J.P., Lafossae, A., Sims, T.J., Grynpas, M. & Bailey, A.J. (2002). Cross-link profile of bone collagen correlates with structural organization of trabeculae. *Bone* **31**(1): 70 76.

Bauer, J.S. & Link, T.M. (2009). Advances in osteoporosis imaging. *European Journal of Radiology* **71**: 440-449.

Bennett, K.A. & Osborne, R.H. (1986). Interobserver reliability in anthropometry. *Human Biology* **58**(5): 751-759.

Bi, H., Chen, X., Gao, S., Yu, X., Xiao, J., Zhang, B., Liu, X. & Dai, M. (2017). Key triggers in osteoclast-related diseases and available strategies for targeted therapies: A review. *Frontiers in Medicine* **4**: 1-10.

Bland J.M. & Altman D.G. (1986). Statistical methods for assessing agreement between two methods of clinical measurement. *Lancet*, **1**: 307-310.

Boivin, G. & Meunier, P.J. (2002). Changes in bone remodelling rate influence the degree of mineralization of bone. *Connective Tissue Research* **43**: 2-3.

Bolliger, S.A., Thali, M. J., Ross, S., Buck, U., Naether, S. & Vock, P. (2008). Virtual autopsy using imaging: Bridging radiologic & forensic sciences. A review of the Virtopsy and similar projects. *European Radiology* **18**:273-282.

Bouxsein, M.L., Boyd, S.K., Christiansen, B.A., Guldberg, R. E., Jepsen, K.J. & Müller, R. (2010). Guidelines for assessment of bone microstructure in rodents using micro-computed tomography. *Journal of Bone Mineral Research* **25**(7): 1468 – 1486.

Brenner, D.J. & Hall, E.J. (2007). Computed tomography – An increasing source of radiation exposure. *The New England Journal of Medicine* **357**(22): 2277-2284.

Castiglioni, S., Cazzaniga, A., Albisetti, W. & Maier, J.A. (2013). Magnesium and osteoporosis: current state of knowledge and future research directions. *Nutrients* **5**(8): 3022-3033.

Chalmers, P.N. & Chamberlain, A.M. (2017). 'Biomechanics of the elbow' in Tashjian, R.Z. (ed.). *The Unstable Elbow*. Salt Lake City: Springer International Publishing, pp. 13-26.

Chappard, D., Retailleau-Gaborit, N., Legrand, E., Baslé, M.F. & Audran, M. (2005). Comparison insight bone measurements by histomorphometry and µCT. *Journal of Bone and Mineral Research* **20**(7): 1177-1184.

Clarke, B. (2008). Normal bone anatomy and physiology. *Clinical Journal of the American Society of Nephrology* **3**(3): S131-139.

Compston, J. (2006). Bone quality: what is it and how is it measured? *Arquivos Brasileiros de Endocrinologia & Metabologia* **50**(4): 579-585.

Crockett, J.C., Rogers, M.J., Coxon, F.P., Hocking, L.J. & Helfrich, M.H. (2011). Bone remodelling at a glance. *Journal of Cell Science* **124**: 991-998.

Currey, J.D. (2002). *Bones.* New Jersey: Princeton University Press.

Delmas, P.D. (2000) Markers of bone turnover for monitoring treatment of osteoporosis with antiresorptive drugs. *Osteoporosis International* **11**(Suppl 6): S66-S76.

Diwan, R.K., Rani, A., Chopra, J., Srivastava, A.K., Sharma, P.K., Verma, R.K. & Pankaj, A.K. (2013). Incidence of supratrochlear foramen of the humerus in North Indian population. *Biomedical Research* **24**(1): 142 – 145.

Donnelly, E., Chen, D.X., Boskey, A.L., Baker, S.P. & van der Meulen, M.C.H. (2010). Contribution of mineral to bone structural behaviour and tissue mechanical properties. *Calcified Tissue International* **87**(5): 450-460.

Drake, R., Vogl, A.W. & Mitchell, A. (2019) *Gray's Anatomy for Students* (4th ed.). Edinburgh: Elsevier

Duan, Y., Wang, X.F., Evans, A. & Seeman, E. (2005). Structural and biomechanical basis of racial and sex differences in vertebral fragility in Chinese and Caucasians. *Bone* **36**(6): 987-998.

Eleswarapu, S.V., Responte, D.J. & Athanasiou, K.A. (2011) Tensile properties, collagen content, and crosslinks in connective tissue of the immature knee joint. *Public Library of Science One* **6**(10): e26178. https://doi.org/10.1371/journal.pone.0026178.

Fonseca, H., Moreira-Gonçalves, D., Coriolano, H.J.A. & Duarte, J.A. (2014). Bone quality: the determinants of bone strength and fragility. *Sports Medicine* **44**(1): 37 -53.

Glanville E.V. (1967). Perforation of the coronoid-olecranon septum. Humero-ulnar relationships in Netherlands and African populations. *American Journal of Physical Anthropology* **26**: 85-92.

Goto, R. & Mascie-Taylor, C.G.N. (2007). Precision of measurement as a component of variance. *Journal of Physical Anthropology* **26**(2): 253-256.
Churchill Livingstone.

Griffith, J.F. & Genant, H.K. (2011). New imaging modalities in bone. *Current Rheumatology Reports* **21**: 241-250.

Hancox, N.M. (1972). *Biology of Bone.* Cambridge: Cambridge University Press.

Hirayama, T., Danks, L., Sabokbar, A. & Athanasou, N.A. (2002). Osteoclast formation and activity in the pathogenesis of osteoporosis in rheumatoid arthritis. *Rheumatology* **41**: 1232-1239.

Hirsh, I.S. (1927). The supratrochlear foramen: Clinical and anthropological considerations. *American Journal of Surgery* **2**: 500-505.

Hoaglin, D.C. & Iglewicz, B. (1987). Fine tuning some resistant rules for outlier labeling. *Journal of American Statistical Association* **82**: 1147-1149.

Hogg, R.V. & Tanis, E.A. (2001). *Probability and statistical inference* (5th ed.). New Jersey: Prentice Hall.

Jiang, Y., Zhao, J., Liao, E.Y., Dai, R.C., Wu, X.K. & Genant, H.K. (2005). Application of micro-CT assessment of 3-D bone microstructure in preclinical and clinical studies. *Journal of Bone Mineral Metabolism* 25(1): 122-131.

Kak, A.C. & Slaney, M. (1999). *Principles of Computerized Tomographic Imaging.* New York: The Institute of Electrical and Electronics Engineers.

Kapandji, I. A. (1982). *The Physiology of the Joints: Volume One Upper Limb* (5th ed.). New York: Churchill Livingstone.

Kim, M.H. & Kim, J.S. (2003). The Relationship Between Body Composition and Bone Mineral Density in College Women. *Journal of Korean Academy of Nursing* **33**(3):312-320.

Kimura, S., Sasase, T., Ohta, T., Sato, E., Matsushita, M. (2012). Characteristics of bone turnover, bone mass and bone strength in Spontaneously Diabetic Torii-*Lepr*^{fa} rats. *Journal of Bone Mineral Metabolism* **30**: 312 – 320.

Kierszenbaum, A.L. & Tres, L.L. (2012). *Histology and cell biology: An introduction to pathology*, (3rd ed). Philadelphia, PA: Saunders.

Kirchhoff, C., Braunstein, V., Milz, S., Sprecher, C.M., Kirchhoff, S., Graw, M., Imhoff, A.B. & Hinterwimmer, S. (2012). Age and gender as determinants of the bone quality of the greater tuberosity: A HR-pQCT cadaver study. *BMC Musculoskeletal Disorders* **13**(221): 1-8.

Kramer, B. & Allan, J.C. (2005). *Fundamentals of Human Osteology.* Durban, South Africa: LexisNexis Butterworths.

Krishnamurthy, A., Yelicharla, A.R., Takkalapalli, A., Munishamappa, V., Bovinndala, B. & Chandramohan, M. (2011). Supratrochlear foramen of the humerus – a morphometric study. *International Journal of Biological and Medical Research* **2**(3): 829 – 831.

Koyun, N., Aydinlioglu, A. & Gumrukcuoglu, F.N. (2011). Aperture in coronoid-olecranon septum:

A radiological evaluation. *Indian Journal of Orthop*aedics **45**:392 – 395.

Kumar, R. & Hans, S. (2016) Filtered back projection algorithm on computed tomography (CT) scan. *International Research Journal of Engineering and Technology* **3**(6): 2152-2156.

Lieben, L. & Carmeliet, G. (2013). Vitamin D signalling in osteocytes: effects on bone and mineral homeostasis. *Bone* **54**(2): 237-234.

Lin, L.I.K. (1989) A concordance correlation coefficient to evaluate reproducibility. *Biometrics* **45**(1):255-268.

Lin, L. & Torbeck, L.D. (1998). Coefficient of accuracy and concordance correlation coefficient: new statistics for methods comparison. *PDA Journal of Pharmaceutical Science and Technology* **52**(2): 55-59.

Lefèvre, V., Ravi-Chandar, K. & Lopez-Pamies, O. (2015). Cavitation in rubber: an elastic instability or a fracture phenomenon? *International Journal of Fracture* **192**(1): 1-23.

Leidig-Bruckner, G., Grobholz, S., Bruckner, T., Scheidt-Nave, C., Nawroth, P. & Schneider, J.G. (2014). Prevalence and determinants of osteoporosis in patients with type 1 and type 2 diabetes mellitus. *BioMed Central* **14**:33.

Lorenzo, J. (2000). Interactions between immune and bone cells: new insights with many remaining questions. *The Journal of Clinical Investigation* **106**(6): 749-752.

Lu, T.W. & Chang, C.F. (2012). Biomechanics of human movement and its clinical applications. *The Kaohsiung Journal of Medical Sciences* **28** (2 Suppl.): S13-S25.

Mahajan, A. (2011). Supratrochlear foramen: Study of humerus in North Indians. *Professional Medical Journal* **18**: 128 – 132.

Marieb, E.N. (2009) *Essentials of Human Anatomy and Physiology* (10th ed.). USA: Pearson.

Mays, S. (2008). Septal aperture of the humerus in a Mediaeval human skeletal population. *American Journal of Physical Anthropology* **136**: 432 – 440.

McClanahan, B.S., Harmon-Clayton, K., Ward, K.D., Klesges, R.C., Vukadinovich, C.M. & Cantler, E.D. (2002). Side-to-side comparisons of bone mineral density in upper and lower limbs of collegiate athletes. *Journal of Strength and Conditioning Research* **16**(4): 586-590.

Miedel, E.L., Brisson, B.K., Hamilton, T., Geason, H., Swain, G.P., Lopas, L., Dopkin, D., Perosky, J.E., Kozloff, K.M., Hankenson, K.D. & Volk, S.W. (2015). Type III collagen modulates fracture callus formation and early remodelling. *Journal of Orthopaedic Research* **33**(5): 675-684.

Ming-Tzu, P. (1935). Septal apertures in the humerus in the Chinese. *American Journal of Physical Anthropology* **20**(2): 165 – 170.

Moores, A. (2006). Humeral condylar fractures and incomplete ossification of the humeral condyle in dogs. *In Practice* **28**: 391 – 397.

Morrey, B.F. & An, K.N. (2005). Stability of the elbow: Osseous constraints. *Journal of Shoulder and Elbow Surgery* **14** (1) Suppl: S174-S178.

Morrey, B.F. Llusá-Pérez, M. & Ballesteros-Betancourt, J.R. (2018). 'Anatomy of the Elbow Joint' in Morrey, B.F., Sanchez-Sotelo, J. & Morrey, M.E. (eds.). *Morrey's the elbow and its disorders.* Philadelphia: Elsevier, pp 9-32.

Myszka, A. & Trzcinski, D. (2015). Septal aperture and osteoarthritis – The same or independent origins? *Advances in Anthropology* **5**: 116-121.

Nair, A.K., Gautieri, A., Chang, S.W. & Buehler, M.J. (2013). Molecular mechanics of mineralized collagen fibrils in bone. *Nature Communications* **4**: 1-9.

Nayak, S.R., Das, S., Krishnamurthy, A., Prabhu, L.V. & Potu, B.K. (2009). Supratrochlear foramen of the humerus: A anatomico-radiological study with clinical implications. *Upsala Journal of Medical Sciences* **114**: 90-94.

Ndou, R., Smith, P., Gemell, R. & Mahatla, O. (2013). The supratrochlear foramen of the humerus in a South African dry bone sample. *Clinical Anatomy* **26**: 870 – 874.

Ndou, R. & Schepartz, L.A. (2016). Morphometric characteristics of the humerus and ulna in limbs bearing the supratrochlear aperture (STA). *The Anatomical Record* **299**: 220-233.

Ndou, R., Pillay, S. & Schepartz, L.A. (2018). Characterization of the tissue crossing the supratrochlear aperture of the humerus using histological techniques. *Surgical and Radiologic Anatomy* **40**(12): 1371-1377.

Nieves, J.W., Formica, C., Ruffing, J., Zion, M., Garrett, P., Lindsay, R. & Cosman, F. (2005). Males have larger skeletal size and bone mass than females, despite comparable body size. *Journal of Bone and Mineral Research* **20**(3): 529-535.

Oei, L., Zillikens, M.C., Dehghan, A., Buitendijk, G.H.S., Castano-Betancourt, M.C., Estrada, K., Stolk, L., Oei, E.H.G., van Meurs, J.B.J., Janssen, J.A.M.J.L., Hofman, A., van Leeuwen, J.P.T.M., Witteman, J.C.M., Pols, H.A.P., Uiterlinden, A.G., Klaver, C.C.W., Franco, O.H. & Rivadeneira, F. (2013). High bone mineral density and fracture risk in type 2 diabetes as skeletal complications of inadequate glucose control. *Diabetes Care* **36**(6): 1619 – 1628.

Papaloucas C., Papaloucas M. & Stergioulas A. (2011). Rare Cases of Humerus Septal Apertures in Greeks. *Trends in Medical Research*, **6**(3): 178–83

Paraskevas, G.K., Papaziogas, B., Tzaveas, A., Giaglis, G., Kitsoulis, P. & Natsis, K. (2010). The supratrochlear foramen of the humerus and its relation to the medullary canal: A potential surgical application. *Medical Science Monitor* **16**(4): BR119 – BR123.

Paraskevas, G.K., Natsis, K., Anastasopoulos, N., Ioannidis, O. & Kitsoulis, P. (2012). Humeral septal aperture associated with supracondylar process: a case review of the literature. *Italian Journal of Anatomy and Embryology* **117**(3): 135 – 141.

Parfitt, A.M., Mathews, C.H.E., Villanueva, A.R. & Kleerekoper, M. (1983). Relationships between surface, volume, and thickness of iliac trabecular bone in aging and in osteoporosis. *Journal for Clinical Investigation* **72**: 1396-1409.

Park, H.M. (2009). *Comparing group means: T-test and one-way ANOVA using STATA, SAS, R and*

SPSS. Working paper. The University Information Technology Services (UITS). Centre for Statistical and Mathematical Computing, Indiana University, http://www.indiana.edu/~statmath/stat/all/ttest.

Parra-Torres, A.Y., Valdes-Flores, M., Orozco, L. & Velazquez-Cruz, R. (2013). Molecular aspects of bone remodelling. *InTech* 1 – 27.

Patel, S.V., Sutaria, L.K., Nayak, T.V., Kanjiya, D.P., Patel, B.M. & Aterkar, S.H. (2013). Morphometric study of the supratrochlear foramen of humerus. *International Journal of Biomedical and Advance Research* **4**(2): 89 – 92.

Paternoster, L., Lorentzon, M., Lehtimäki, T., Eriksson, J., Kähönen, M., Raitakari, O., et al. (2013). Genetic Determinants of Trabecular and Cortical Volumetric Bone Mineral Densities and Bone Microstructure. Public Library of Science Genetics 9(2): e1003247. https://doi.org/10.1371/journal.pgen.1003247

Paulsen D.F. (2010). Connective Tissue. In: *Histology & cell biology: Examination & Board Review*, (5th ed.). New York: The McGraw-Hill Companies.

Qiu, S., Rao, D.S., Fyhriye, D.P., Palnitkar, S. & Parfitt, A.M. (2005). The morphological association between microcracks and osteocyte lacunae in human cortical bone. *Bone* **37**(1): 10-15.

Raggatt, L.J. & Partridge, N.C. (2010). Cellular and molecular mechanisms of bone remodeling. *Journal of Biological Chemistry* **285**:25103-25108.

Retsky, M. (2008). Electron beam computed tomography: challenges and opportunities. *Physics Procedia* **1**: 149-154.

Rho, J. Y., Ashman, R. B., & Turner, C. H. (1993). Young's modulus of trabecular and cortical bone material: ultrasonic and microtensile measurements. *Journal of Biomechanics* **26**: 111-119.

Riggs, C.M., Vaughan, L.C., Evans, G.P., Lanyon, L.E. & Boyde, A. (1993). Mechanical implications of collagen fibre orientation in cortical bone of equine radius. *Anatomy and Embryology* **187**(3): 239-248.

Rooker, J.C., Smith, J.C.A. & Amirfeyz, R. (2016). Anatomy, surgical approaches and biomechanics of the elbow. *Orthopaedics and Trauma,* http://dx.doi.org/10.1016/j.morph.2016.05.008

Ruff, C.B. & Hayes, W.C. (1988). Sex differences in age-related remodelling of the femur and tibia. *Journal of Orthopaedic Research* **6**(6): 886-896.

Ruff C, Holt B, Trinkaus E. (2006). Who's afraid of the big bad Wolff?:"Wolff's law" and bone functional adaptation. *American Journal of Physical Anthropology* **129**:484-498.

Schindeler, A., McDonald, M.M., Bokko, P. & Little, D.G. (2008). Bone remodelling during fracture repair: The cellular picture. *Seminars in Cell & Developmental Biology* **19**(5): 459-466.

Schult, T.M.K., Ensrud, K.E., Blackwell, T., Ettinger, B., Wallace, R. & Tice, J.A. (2004). Effect of isoflavones on lipids and bone turnover markers in menopausal women. *Maturitas* **48**(3): 209

- 218.

Seeman, E. & Delmas, P.D. (2006). Bone quality – The material and structural basis of bone strength and fragility. *The New England Journal of Medicine* **354**: 2250-2261.

Shibata, Y., Fujita, S., Takahashi, H., Yamaguchi, A. & Koji, T. (2000). Assessment of decalcifying protocols for detection of specific RNA by non-radioactive in situ hybridization in calcified tissues. *Histochemistry and Cell Biology* **113**: 153 – 159.

Singhal S. & Rao, V. (2007). Supratrochlear Foramen of the Humerus. *Anatomical Science International* 82:105-107.

Sundh, D., Nilsson, A.G., Nilsson, M., Johansson, L., Mellström, D. & Lorentzon, M. (2017). Increased cortical porosity in women with hip fracture. *Journal of Internal Medicine* **281**(5): 496 506.

Teitelbaum, S.L. (2000). Bone resorption by osteoclasts. *Science* **289**(5484): 1504 – 1508.

Thompson, D.D. (1980). Age changes in bone mineralization, cortical thickness, and Haversian canal area. *Calcified Tissue International* **31**: 5 – 11.

Thomsen, J.S., Laib, A., Koller, B., Prohaska, S., Mosekilde, L. & Gowin, W. (2005). Stereological measures of trabecular bone structure: comparison of 3D micro computed tomography with 2D histological sections in human tibial bone biopsies. *Journal of Microscopy* **218** (2): 171-179.

Trotter, M. (1934). Septal apertures in the humerus of American whites and negroes. *American Journal of Physical Anthropology* **14**(2): 213 – 227.

Ushiki, T. (1992). The three-dimensional ultrastructure of the collagen fibers, reticular fibers and elastic fibers: a review. *Kaibogaku Zasshi* **67**(3): 186-199.

Ushiki, T. (2002). Collagen fibers, reticular fibers and elastic fibers. A comprehensive understanding from a morphological viewpoint. *Archives of Histology and Cytology* **65**(2): 109 – 126.

Van Der Linden, J.C., Verhaar, J.A.N. & Weinans, H. (2001). A three-dimensional simulation of age related remodelling in trabecular bone. *Journal of Bone and Mineral Research* **16**(4): 688 696.

van Driel, M. & van Leeuwen, J.P.T.M. (2017). Vitamin D endocrinology of bone mineralization. *Molecular and Cell Endocrinology* **453**: 46-51.

Viguet-Carrin, S., Garnero, P. & Delmas, P.D. (2006). The role of collagen in bone strength. *Osteoporosis International* **17**: 319-336.

Wang, X.F., Duan, Y., Beck, T.J. & Seeman, E. (2005). Varying contributions of growth and ageing to racial and sex differences in femoral neck structure and strength in old age. *Bone* **36**(6): 978-986.

Wainwright, S.A., Biggs, W.D., Currey, J.D., Gosline, J.M. (1982). *Mechanical design in organisms.* New Jersey: Princeton University Press.

Yao, X., Carleton, S.M., Kettle, A.D., Melander, J., Phillips, C.L. & Wang, Y. (2013). Gender

dependence of bone structure and properties in adult osteogenesis imperfecta murine model. *Annals of Biomedical Engineering* **41**(6): 1139-1149.

Appendices

Appendix A: Reagents and equipment used

Reagents

- Formaldehyde (Associated Chemicals Enterprise, Johannesburg, RSA)
- Mayer's solution (SAAR2422001LC, Merck Chemicals (Pty.) Ltd., Gauteng, RSA)
- Eosin yellowish (SAAR2186000DC, Merck Chemicals (Pty.) Ltd., Gauteng, RSA)
- Potassium di-hydrogen orthophosphate (CAS No. 7778-77-0, Associated Chemicals Enterprise, Johannesburg, RSA)
- Potassium chloride (CAS No. 7447-40-7, Associated Chemicals Enterprise, Johannesburg, RSA)
- di-Sodium hydrogen orthophosphate anhydrase (CAS No. 7558-79-4, Associated Chemicals Enterprise, Johannesburg, RSA)
- Sodium chloride (CAS No. 7647-14-5, Associated Chemicals Enterprise, Johannesburg, RSA)
- Sodium hydrogen carbonate (CAS No. 582-28-20, Saarchem (Pty.) Ltd., Krugersdorp, RSA)
- tri-Sodium Citrate dehydrate (CAS No. 6132-04-3, Associated Chemicals Enterprise, Johannesburg, RSA)
- 3-aminopropyl tri-ethoxy silane (1010666628, Sigma Aldrich, Steinheim, Germany)
- Acetone (SAAR1022040LC, Merck Chemicals (Pty.) Ltd., Gauteng, RSA)
- Ammonium Oxylate (Catalog No. 1046946, Merck Chemicals (Pty.) Ltd., Gauteng, RSA)
- Formic Acid (Catalog no. 1041684, Merck Chemicals (Pty.) Ltd., Gauteng, RSA)
- Xylene (CAS No. 108-38.3, Associated Chemicals Enterprise, Johannesburg, RSA)
- Entellen (HX 088232, Merck RGaA, Darmstadt, Germany)
- Hydrochloric acid 1% (Associated Chemicals Enterprise, Johannesburg, RSA)
- Tween 20 (616-45-00KF, Saarchem, Wadeville, Gauteng, RSA)
- dodeca-Tungstophospheric Acid (SAAR6142000DC Merck Chemicals (Pty.) Ltd., Gauteng, RSA)
- Orange G (C.I 16230) (CAS No. 1936-15-8 Merck KGaA, Darmstadt Germany)
- Aniline Blue, WS (C.I. 42780) (Fisher Scientific Company, New Jersey USA)
- Acid Fuschin (C.I. 42685) (CAS No. 3244-88-0 Merck KGaA, Darmstadt Germany)
- Pelikan Fount India (Pelikan, Germany)

Equipment

- ARIBEX NOMAD® CE eXaminer
- Automatic tissue processor (Shandon, Citadel 1000)
- Embedding table (Miles scientific, serial number 31602-554)
- Weighing scales:
    - (Model – KERN EW600-2M, Serial No. 8423167, Albstadt, Germany)
    - Model – SARTORIUS GMBH, Fabr. No. 36020123)
- Incubator (Model-508-2U, Labcon shaker)
- ESCO Laboratory fume hood (Model: EFA-4UDW-8, Serial 2011-60070)
- Microtome (Leica RM 2125RM, Fabr. No. 07390329)
- Microscope (Axioscope) (Model: Axiocom HRC, Identification number 105-041756)
- Olympus BX63 Fluorescence Microscope
- Microfocus computed tomography (µCT) X-ray machine (NIKON XTH 225/320 LC)

Software packages

- Microsoft Excel 2016 (Microsoft Corporation)
- IBM SPSS version 24
- Volume Graphics Studio version 3.0 software
- Axiovision (AXIOVs) version 4.7.2.0 (Carl Zeiss Microscopy)
- Olympus CellSens™
- ImageJ®

Appendix B – 10% neutral buffered formalin

100ml	Formalin (37-40% stock solution)
900ml	Distilled water
4g/L	NaH_2PO_4 (monobasic)
6.5g/L	Na_2HPO_4 (dibasic/ anhydrous)

Appendix C – 10% Formic citric acid decal fluid and saturated ammonium oxylate

10% Formic citric acid

450ml	Formic Acid
5050ml	Distilled water
400ml	HCl
50g	Tri-Sodium Citrate

Saturated ammonium oxylate

200ml	Distilled water
2mg	Ammonium oxylate crystals (at a time)

Allow the solution to mix. Add another spoon of Ammonium oxalate crystals until it can no longer be dissolved.

For decalcification:

1. Pour 10% Neutral Buffered Formalin into a waste container
2. Rinse the specimen in tap water (twice)
3. Pour 30ml of Formic Citric Acid into the bijou bottle
4. Leave to decalcify overnight
5. Extract 1ml of formic citric acid from each bijou bottle into a test tube
6. Put 1ml of saturated ammonium oxalate in each tube. If the solution turns white immediately then continue with decalcification. If not allow the solution to stand for 10 minutes to ensure no traces of calcium are found i.e. the solution is clear.
7. Rinse the specimen in running water for 30 minutes and store in 10% NBF until processing

Appendix D - Tissue processing

The tissue was processed using an automatic tissue processor (Shandon citadel 1000) as follows:

1. 10% buffered formalin for 4 hours
2. 70% alcohol for 1 hour
3. 95% alcohol for 2 hours
4. 95% alcohol for 2 hours
5. 95% alcohol for 2 hours
6. 95% alcohol for 2 hours
7. 100% alcohol for 2 hours
8. 100% alcohol for 2 hours
9. 100% alcohol for 2 hours
10. Chloroform for 2 hours
11. Chloroform for 2 hours
12. Wax for 2 hours
13. Wax for 2 hours

Appendix E – Haematoxylin and Eosin staining procedure

Haematoxylin

4g	Haematoxylin
1000ml	Distilled water
0.3g	Sodium Iodate
50g	Potassium Alum
1.5g	Citric Acid
75g	Chloral Hydrate

Eosin

Stock:

8g	Eosin Y
2g	Erythrocin
1000ml	Distilled water

Working solution:

250ml	Stock Eosin
20g	Calcium chloride
750ml	Distilled water

Method

1. Dewax and hydrate sections
2. Stain in Mayer's Haematoxylin for 20 minutes
3. Wash in tap water for 5 minutes
4. Differentiate by dipping in 1% Alcohol once
5. Blue the slides by running in tap water for 5 minutes
6. Counterstain in Eosin for 10 minutes
7. Wash briefly in running water
8. Dehydrate slides through alcohol grades and then into Xylene
9. Mount with Entellan, coverslip and leave to dry

Appendix F – Rapid one-step Mallory Heidenhain staining procedure

Solution:

200ml Distilled water

Dissolve each of the following before adding the next stain:

1.0g Phosphotungstic acid

2.0g Orange G (C.I 16230)

1.0g Aniline Blue, WS (C.I 42780)

3.0g Acid Fuchsin (C.I 42685)

Method:

1. Deparaffinize and hydrate sections to water
2. Stain slides in staining solution for 20 minutes
3. Wash in running tap water for 5 minutes
4. Rapidly dehydrate in 100% alcohol for 10 seconds
5. Immerse in Xylene for 5 minutes
6. Dry by blotting overnight
7. Mount using Entellen and allow to dry

Appendix G – Picrosirius red staining procedure

Solutions

1. Picrosirius Red
    a. 0.5g Sirius Red F3B
    b. 500ml Saturated aqueous solution of picric acid
2. Toluidine Blue
    a. 0.5g Toluidine Blue
    b. 100ml distilled water pH 1 – 1.5
3. 6% Nitric Acid
    a. 6ml of Nitric Acid in 94ml of distilled water

Let the solution stand for 24 hours before use.

Procedure

1. Incubate sections in two changes of xylene, two changes of 100% alcohol and one change of 95% alcohol (5 minutes each)
2. Wash in running tap water for 5 minutes
3. Pre-treat in 6% Nitric Acid for 5 minutes
4. Stain in Toluidine Blue for 10 minutes
5. Wash in distilled water for 10 seconds until Toluidine Blue is out
6. Stain with Picrosirius Red for 5 minutes
7. Wash in distilled water briefly
8. Blot dry
9. Pass through one change of 95% alcohol, 2 changes of 100% alcohol and 2 changes of xylene before mounting the coverslip with entellen.

Appendix H – Anterior vs. posterior measurement gradient on ImageJ

The following Macro was created to divide the rectangular plots into 5 equal squares:

```
macro "cut into fifths horizontally" {
  roiManager("Add");
  firstROI = roiManager("count")-1;
  getSelectionBounds(x, y, width, height);
  fifth = height / 5;
  for (i=0; i<5; i++) {
    makeRectangle (x, y+(i*fifth), width, fifth);
    roiManager("Add");
    roiManager("select", roiManager("count")-1);
    roiManager("rename", "rectangle");
    roiManager("select", newArray(firstROI, roiManager("count")-1));
    roiManager("and");
    roiManager("Add");
    roiManager("deselect");
    roiManager("select", roiManager("count")-2);
    roiManager("delete");
  }
}
```

Appendix I – Analysis on VG Studio Max

1. Open VG Studio Max 3.0
2. File
    a. Import
    b. VGI volume
    c. Browse
    d. Open file
    e. Next
3. Histogram
    a. Move the red line to the beginning of the first peak (if 3 or more peaks then move the red vertical line between 1st and 2nd peaks)
    b. Select "Hide"
    c. Select "preview" – screenshot
    d. Check projections to make sure all bone is included, reduced the container space.
    e. Finish
4. Play around with histogram on the bottom right-hand side to make the images clearer (move the diagonal line)
5. 4 screens appear with different views to isolate, scroll on different views
6. To do osteometric measurements
    a. Instruments
    b. Calliper
    c. Drag calliper from beginning to endpoint for length – proximal and distal divide length by 4
    d. To save an image
        i. File
        ii. Save image
        iii. Change the view to select only the image needed
7. Surface determination and ROI
    a. On left-hand panel select ROI from surface (red box)
    b. Region growing (Wand)
    c. Double click on ROI
    d. Click big red box on pop-up dialogue – region 1 should show up on top right-hand dialogue box
    e. Erodilate dialog pop-up
        i. Mode = opening/closing
        ii. Radius = 9
        iii. Click on image (should change colour)
        iv. Click on the small red box
        v. Repeat process; or
        vi. Click on the pencil to make sure all bone is included – erase whatever is not necessary
        vii. Click on the small red box
        viii. Erodilate
        ix. Radius = 9
        x. Small box
        xi. Close dialogue
    f. Object

g. Properties
h. Morphometrics
i. Update – take all necessary measurements (Screenshot)

All images saved as a .tif

Appendix J – Ethics Waiver

cc Alison

University
of the Witwatersrand,
Johannesburg

Human Research Ethics Committee (Medical)
(formerly Committee for Research on Human Subjects (Medical)

Secretariat: Research Office, Room SH10005, 10th floor, Senate House • Telephone: +27 11 717-1234 • Fax: +27 11 339-5708
Private Bag 3, Wits 2050, South Africa

Ref: W-CJ-101109-1

09/11/2010

TO WHOM IT MAY CONCERN:

Waiver: This certifies that the following research does not require clearance from the Human Research Ethics Committee (Medical).

Investigator: **School of Anatomical Sciences (Head: Prof T J M Daly).**

Project title: **Research on cadaveric material.**

Reason: In terms of Chapter 8, sections 62-64 of the National Health Act No 61 of 2003 donated bodies and their tissues may be used for, among other purposes, health research. Use of such material is subject only to permission from the responsible person in the School of Anatomical Sciences - the Head or person designated by the Head.

UNIVERSITY OF THE WITWATERSRAND
PROF PE CLEATON-JONES
HREC (MEDICAL)
2010 -11- 09
JOHANNESBURG

Professor Peter Cleaton-Jones
Chair: Human Research Ethics Committee (Medical)

copy: Anisa Keshav, Research Office, Senate House, Wits

Appendix K – Turn-it-in report

481830:Shayla_Pillay_481830_Turnitin.docx

ORIGINALITY REPORT

20%	7%	4%	16%
SIMILARITY INDEX	INTERNET SOURCES	PUBLICATIONS	STUDENT PAPERS

PRIMARY SOURCES

1	Submitted to University of Witwatersrand Student Paper	14%
2	www.cnic.ac.cn Internet Source	3%
3	link.springer.com Internet Source	2%
4	asbmr.onlinelibrary.wiley.com Internet Source	2%

Exclude quotes	On	Exclude matches	< 1%
Exclude bibliography	On		